nature communications

Article

https://doi.org/10.1038/s41467-025-67542-6

Dysregulated hippocampal fatty acid metabolism following intermittent hypoxemia-induced neonatal brain injury is rescued by treatment with acetate

Received: 21 November 2024

Accepted: 3 December 2025

Published online: 14 December 2025

Check for updates

Regina F. Fernandez[1,2], Wedad Fallatah[2,3], Yuanyuan Ji[4], Jace W. Jones[4], Cole C. Johnson[5], Caitlin M. Tressler[5], Kristine Glunde[5,6], Rida Ali[1], Ann B. Moser[3], Michael J. Wolfgang[7], Susanna Scafidi[8] ✉ & Joseph Scafidi[1,2,9] ✉

The brain is a lipid-rich organ that experiences rapid growth and development after birth in a period hallmarked by extensive lipid synthesis. We still lack a fundamental understanding of lipid metabolism during this critical time of brain development and how these dynamics occur in infants born extremely preterm (<28 weeks of gestation) suffering from brain injuries. Using an established model of neonatal brain injury due to intermittent hypoxemia, we recapitulate hippocampal-dependent cognitive impairments and examine the extent of changes in the brain's lipid profile. Our results show changes in hippocampal lipid composition and abnormal fatty acid profile. Furthermore, we provide evidence of an increase in mitochondrial fatty acid β-oxidation, a process that is not classically thought of occurring in the developing brain. We find that a specific alternative fuel, acetate, spares fatty acids from mitochondrial β-oxidation. Here, we show that treatment with acetate in vivo in the form of glycerol-triacetate promotes functional recovery and restores hippocampal fatty acid profile after neonatal brain injury.

The developing brain undergoes rapid and complex changes, creating the foundation for a life of cognitive processing. During the third trimester and first year of life, large quantities of fatty acids are required as building blocks to make complex lipids, which in turn, build a lipid-rich brain architecture[1,2]. Thus, this period is characterized by both significant uptake and de novo synthesis of fatty acids in the brain. In contrast, mitochondrial β-oxidation, the other major fate of fatty acids, is negligible, especially compared to the adult brain[3,4]. It remains unknown whether these processes – fatty acid synthesis and oxidation – are dysregulated in neonates born extremely preterm (EPT; <28 weeks of gestation).

Neonatal brain injury is a major contributor to long-term neurodevelopmental delays[5]. It is well documented that nearly all infants born EPT have episodic intermittent hypoxemia (apnea of

[1]The Michael V. Johnston Center for Developmental Neuroscience, Kennedy Krieger Institute, Baltimore, MD, USA. [2]Department of Neurology, Johns Hopkins University School of Medicine, Baltimore, MD, USA. [3]Hugo W. Moser Research Institute, Kennedy Krieger Institute, Baltimore, MD, USA. [4]Department of Pharmaceutical Sciences, University of Maryland, School of Pharmacy, Baltimore, MD, USA. [5]The Russell H. Morgan Department of Radiology and Radiological Science, Division of Cancer Imaging Research, Johns Hopkins University, Baltimore, MD, USA. [6]The Sidney Kimmel Comprehensive Cancer Center, Johns Hopkins University School of Medicine, Baltimore, MD, USA. [7]Department of Physiology, Pharmacology & Therapeutics, Johns Hopkins University School of Medicine, Baltimore, MD, USA. [8]Department of Anesthesiology and Critical Care Medicine, Johns Hopkins University School of Medicine, Baltimore, MD, USA. [9]Department of Pediatrics, Johns Hopkins University School of Medicine, Baltimore, MD, USA. ✉e-mail: sscafid2@jhmi.edu; Scafidi@kennedykrieger.org

prematurity)[6–9]. These brief, repeated episodes (50–100 per day) of apnea lead to low oxygen saturation and are often addressed in the neonatal intensive care unit by providing supplemental O_2 to restore oxygen levels. Unfortunately, these episodes of intermittent hypoxia continue during the entire period until these infants achieve corrected full-term age[7–9]. Clinical observational studies suggest that the frequency, severity, and duration of these episodes impact neurodevelopmental outcomes[8,10]. However, cognitive impacts are often not evident until school age when children confront more complex social and behavioral interactions. Indeed, studies of children born EPT showed impaired executive and cognitive deficits as well as structural changes to the brain (such as lower hippocampal volume)[7–9,11,12]. Both human and animal studies have shown that the hippocampus is vulnerable to injury and hippocampal volume is correlated with memory impairments at childhood[10,12,13].

To study the effects of intermittent hypoxemia, we used a clinically relevant mouse model of neonatal brain injury from apnea of prematurity[14,15]. This model of intermittent hypoxia (IHx) recapitulates the repeated hypoxic episodes from apnea of prematurity observed in human infants born EPT that result in neuroanatomical and neurofunctional deficits[15]. The exact cellular and biochemical mechanisms responsible for impaired memory and learning in children born EPT remain unknown. The timing of preterm brain injury, which coincides with significant uptake and de novo fatty acid synthesis and accretion, suggest that fatty acid metabolism in the developing brain may be implicated. We hypothesize that IHx disrupts hippocampal development by dysregulating fatty acid metabolism. Therefore, our study aimed to delineate the effect of IHx on fatty acid metabolism during the neonatal period.

In this study, using our mouse model of IHx, we recapitulated the long-term hippocampal-dependent cognitive deficits observed in children born EPT and discovered changes in brain lipid metabolism. We report that IHx led to alterations in hippocampal lipid and fatty acid profiles along with increased fatty acid oxidation in astrocytes. This fatty acid oxidation occurred acutely and, interestingly, persisted for several days during the recovery period in normoxia conditions. Fatty acid oxidation was significantly reduced upon exposure to the alternative fuel, acetate. Importantly, in vivo intervention using oral administration of glycerol-triacetate, a clinically feasible source of acetate, rescued hippocampal fatty acids from oxidation, recovered total lipid fatty acid profile, and resulted in improved cognitive deficits.

Results

Injury from intermittent hypoxia alters hippocampal lipid composition

It is established that the first several postnatal days in rodent (approximately postnatal days 0–10) brain development is analogous to the third trimester in human fetal brain development[16,17]. Mice underwent intermittent hypoxemia (IHx) during postnatal days (P) 1–11 and were compared to normoxia controls (Nx) (Fig. 1a). Similar to children born EPT, mice that underwent neonatal IHx (P1-P11) had significantly poor performance on recognition and spatial memory tasks at postnatal day 30 (P30) in both males and females compared to Nx controls (Fig. 1b, c, Supplementary Fig. 1a, b). At P30, the body and brain weight of IHx-injured mice was lower compared to age-matched Nx controls, reflecting the effects of preterm birth on optimal growth in children born EPT (Supplementary Fig. 1c, d)[18–21].

The exact cellular and molecular mechanisms of preterm brain injury are still unknown. EPT and apnea of prematurity occur at a time of extensive lipid synthesis that is concurrent with rapid structural brain growth and development[1,2]. Therefore, we studied brain lipid metabolism, specifically within the hippocampus, in our model of IHx. Within the hippocampus, the percent of total lipids per mg of tissue was not changed at P30 (Fig. 1d, Supplementary Fig. 1e). However, hippocampal lipid profile at this age showed that IHx during the neonatal period altered lipid composition (Fig. 1e–h, Supplementary Table 1). Unsupervised principal component analysis (PCA) showed minimal overlap between groups (Fig. 1e). Subsequent supervised classification by partial least-squares discriminant analysis (PLS-DA), hierarchical clustering, and volcano plot revealed significant differences in lipid classes (Fig. 1f–h, Supplementary Table 1). Specifically, our results show that at P30, 112 lipids were significantly changed in mice that underwent IHx compared to Nx (Fig. 1f–-h, Supplementary Table 1).

The majority of lipids in the brain are synthesized locally via de novo lipogenesis, a process that occurs at high rates during the early neonatal period and declines with age[22–24]. To determine whether de novo lipogenesis was affected by IHx during development, we measured acetate incorporation into hippocampal lipids at several time points (P11, P17, P22, and P30). The results showed that de novo lipogenesis was comparable between Nx and IHx at all ages in both males and females (Supplementary Fig. 1f). Lipids require fatty acids as building blocks, therefore, we explored if there were any changes in total lipid fatty acid composition following IHx at P30 (Fig. 2, Supplementary Tables 2, 3)[2,24–26]. Fatty acid class analysis showed that while saturated fatty acids were comparable between Nx and IHx, the profile significantly differed (Fig. 2c, d). Specifically, the percent of saturated fatty acids composed of a ≥ 20-carbon chain length were decreased following IHx in males and females while C16:0 (palmitate), one of the most abundant saturated fatty acids (~24%), was increased in males only (Fig. 2a, b, e, f, Supplementary Table 2 and 3). The percent of total unsaturated ω−9 fatty acids was significantly decreased after IHx in males only (Fig. 2c, d). Notably, C18:1(n−9) (oleic acid) which constitutes ~15% of total fatty acids, was one of the ω−9 species affected in males (Fig. 2a, Supplementary Table 2). Furthermore, within the ω−9 fatty acid class, the percent of ≥20-carbon long fatty acids were trending towards or significantly decreased in IHx-injured hippocampus in both sexes (Fig. 2e, f). In contrast to the reduced levels of these long and very long-chain fatty acids (VLCFA), the levels of arachidonic acid (C20:4n-6), the essential fatty acid belonging to the ω-6 fatty acid class, was increased in males while no differences were observed in females (Fig. 2a, b, Supplementary Tables 2, 3). Together, these changes in hippocampal lipid composition at P30 in the IHx-injured group reflect prolonged dysregulations in lipid homeostasis during the recovery phase from neonatal intermittent hypoxia.

Next, we investigated whether changes in lipid composition began immediately after the injury and whether they resembled those observed at P30. Hippocampal lipid composition from IHx-injured mice at P11 displayed less changes compared to P30 (Fig. 3a–e, Supplementary Table 4). PCA showed some overlap between P11 Nx and IHx groups (Fig. 3a). Furthermore, PLS-DA revealed that the Nx group was completely separated from the IHx group indicating significant differences in their lipid profile (Fig. 3b). Using hierarchical clustering and volcano plot analysis, we identified the lipid species contributing to the separation of the groups and the direction of their change (Fig. 3c, d, Supplementary Table 4). In contrast to P30, only forty-seven lipids were identified as significantly changed. Phosphatidylserine (PS), the most abundant anionic phospholipid found in brain lipid membranes, was markedly decreased by IHx at P11 and P30 (Figs. 1g, h, 3c–e, Supplementary Tables 1 and 4)[27]. The sum of ceramides was decreased after IHx at P11 but subsequently recovered and exceeded those in the Nx group by P30 (Figs. 1h, and 3c–e, Supplementary Tables 1, 4). We then performed total lipid fatty analysis in the hippocampus at P11 (Fig. 3f–i, Supplementary Fig. 1g, h). In contrast to data at P30, hippocampal levels of long-chain fatty acids at P11 showed minimal changes between Nx and IHx groups (Supplementary Fig. 1g, h and Supplementary Tables 5, 6). Specifically, at P30 we observed significant differences in the levels of palmitate (C16:0) and oleic acid (18:1n−9), while at P11 the levels of these fatty acids were comparable between Nx and IHx in both males and females (Fig. 2a, b, Supplementary Fig. 1g, h,

https://doi.org/10.1038/s41467-025-67542-6

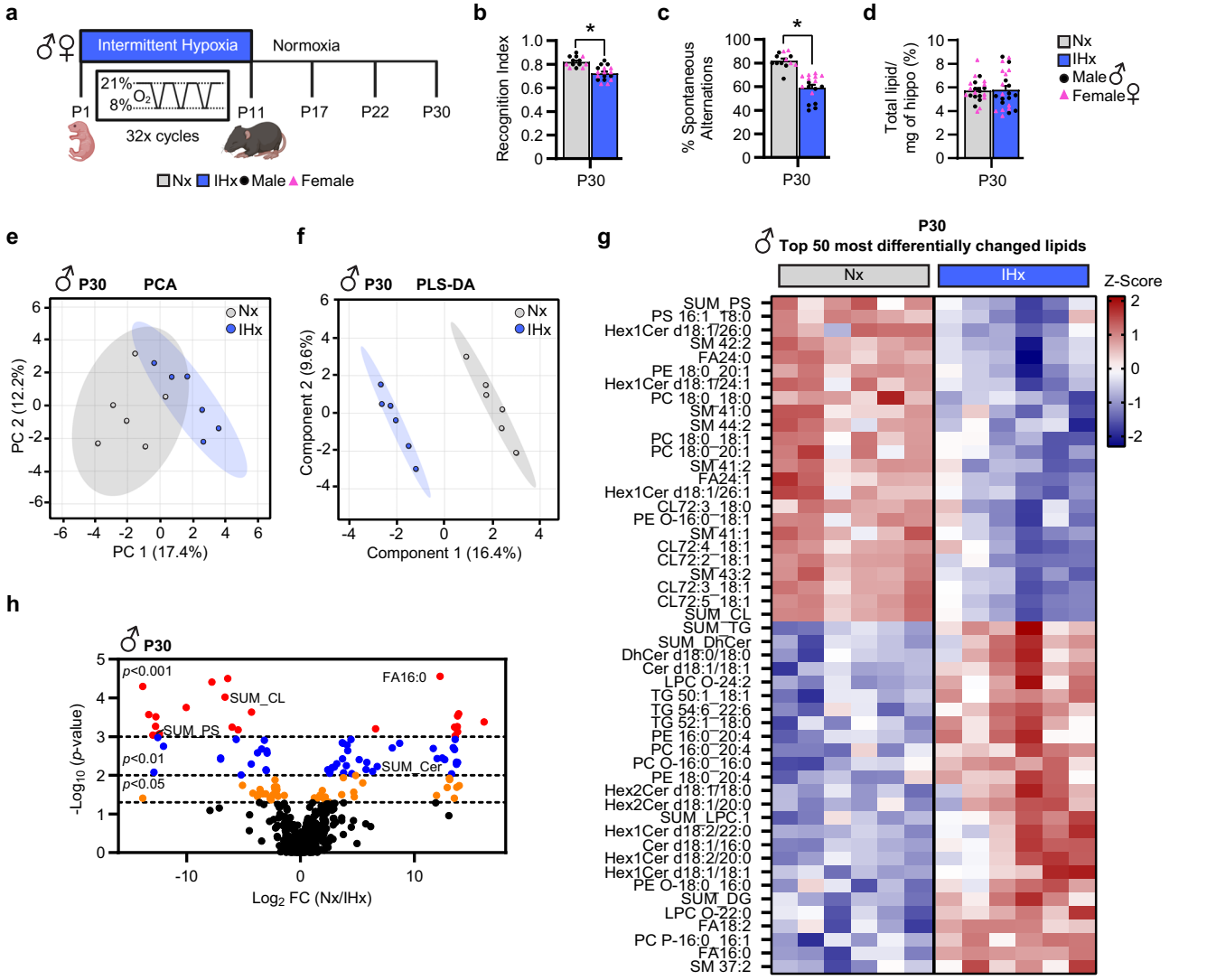

Fig. 1 | Intermittent hypoxia (IHx) alters brain lipid composition in a translational model of neonatal brain injury from apnea of prematurity. a Schematic of IHx protocol. **b** Recognition index on the novel object recognition test after a 12-hour delay for postnatal day (P) 30 Nx and IHx mice (Nx $n = 13$, IHx $n = 17$; biological replicates). **c** Y-Maze % spontaneous alternations of P30 Nx and IHx mice (Nx $n = 13$, IHx $n = 17$; biological replicates). **d** Total lipid extracted per mg of hippocampus expressed as % from P30 Nx and IHx mice (Nx $n = 22$, IHx $n = 24$; biological replicates). **e**–**h** Lipid profiling using liquid chromatography with tandem mass spectrometry (LC-MS/MS) in male Nx and IHx hippocampus at P30 ($n = 6$/group; biological replicates). **e** Principal component analysis (PCA) and (**f**) partial least-squares discriminate analysis (PLS-DA) score plots of lipid profiles comparing Nx and IHx. In (**e**, **f**), elliptical patterns represent 95% confidence intervals. **g** Heatmap of the top 50 most differentially changed lipids between Nx and IHx groups (Distanced measure: Euclidean; clustering algorithm: Ward). **h** Volcano plot depicting changes in lipids species between Nx and IHx groups. Black dots: $p > 0.05$; yellow dots: $0.05 > p > 0.01$; blue dots: $0.01 > p > 0.001$; red dots: $p < 0.001$. The x-axis is log2 (fold change; FC) and the y-axis is −log10 (p-value based on 2-tailed unpaired t-test performed by MetaboAnalyst without adjustments for multiple comparisons). For (**b**–**d**), data are presented as mean ± SEM. Statistical analysis for (**b**–**d**) by unpaired Mann-Whitney 2-tailed test; *$p < 0.05$ (For (**b**, **c**) $p = <0.0001$) Nx vs IHx. **b**–**d** Males, black circles; Females, pink triangles. Cer ceramide, CL cardiolipin, DhCer dihydroceramide, FA fatty acid, HexCer hexosylceramide, Hippo hippocampus, LPC lysophosphatidylcholine, PC phosphatidylcholine, PE phosphatidylethanolamine, PS phosphatidylserine, SM sphingomyelin, TG triacylglycerol. Source data are provided as a Source Data file. Panel (**a**) was created in BioRender. Scafidi, S. (2025) https://BioRender.com/n58a8ts.

Supplementary Tables 2, 3, 5, 6). Similarly, while the percent of ≥20 carbon-long saturated and unsaturated ω-9 fatty acids were decreased at P30 in the IHx group, no such differences were detected at P11 between Nx and IHx groups (Figs. 2e, f and 3h, i).

Next, we evaluated whether the data from murine experiments recapitulate human total lipid fatty acid profile of term human hippocampus (Supplementary Fig. 2). We compared human hippocampal total lipid fatty acid profile to data obtained from Nx controls at P11 and P30 using post-mortem hippocampi from term newborns (Supplementary Fig. 2a–d). This comparison showed compelling similarities to Nx controls at P11 but not at P30 (Supplementary Fig. 2c, d). The rapid brain growth and development is characterized by extensive local synthesis of ≥20 carbon-long saturated fatty acids, which were increased between P11 and P30 Nx mice (P11 - ~0.5% vs P30 - ~2.4%) (Supplementary Fig. 2d). Next, we examined the hippocampal total lipid fatty acid profile between full term (38–40 weeks of gestation) at ~1.6-month-old average postnatal age and extremely preterm infants (≤28 weeks of gestation) at corrected similar age (Supplementary Fig. 2a, e–g, Supplementary Table 7). These results showed that the fatty acid composition of the hippocampus in extremely preterm infants did not differ from those born full term (Supplementary Fig. 2e–g). Moreover, our findings provide evidence that P11 murine hippocampal fatty acid profile correlates to human hippocampus in early infancy (1–3 months) and that the fatty acid results from the

https://doi.org/10.1038/s41467-025-67542-6

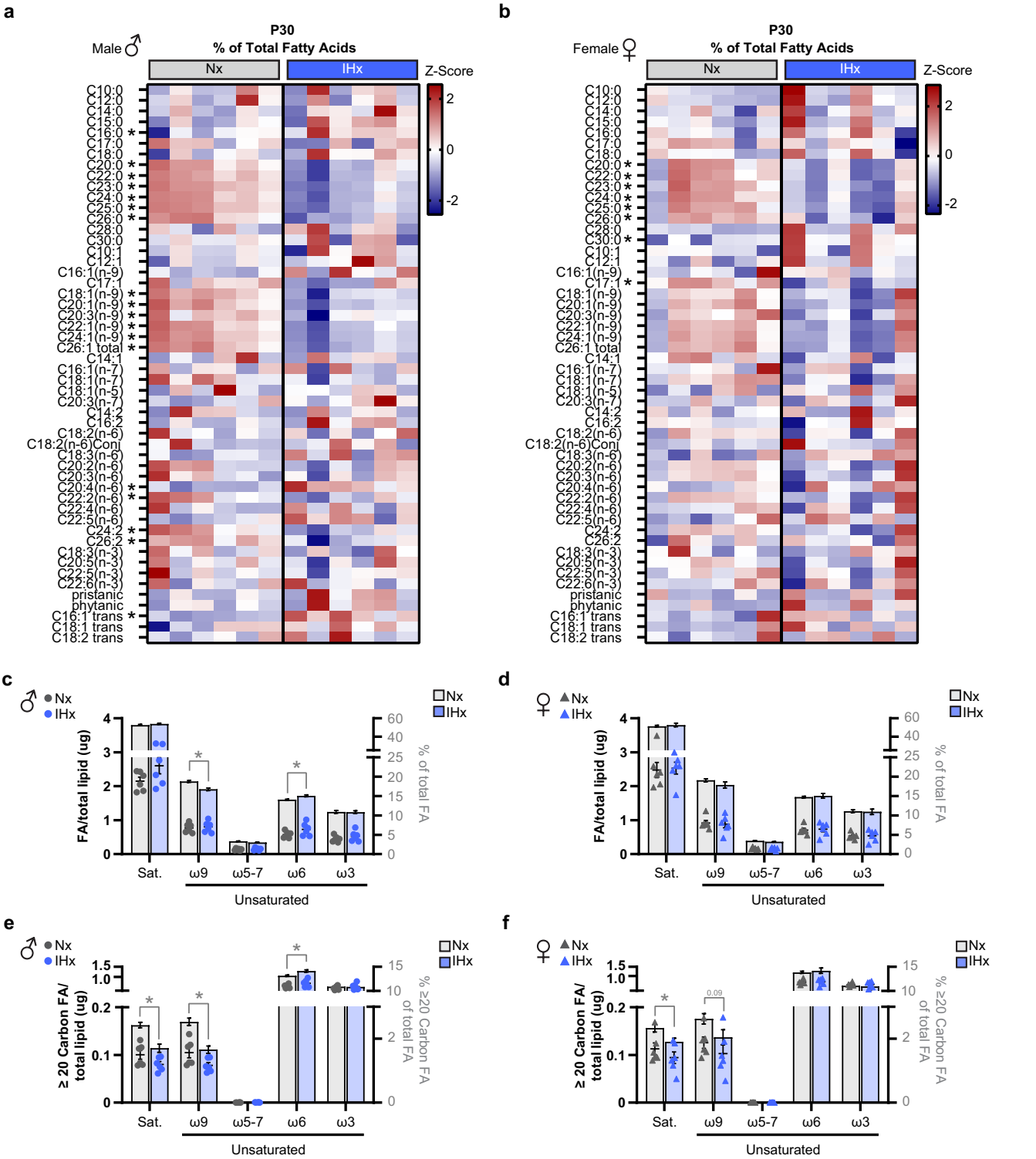

Fig. 2 | IHx results in decreased hippocampal ≥ 20 carbon-long saturated and ω-9 fatty acids at P30. a–**f** Total fatty acids quantified by gas chromatography with tandem mass spectrometry (GC/MS) in (**a**, **c**, **e**) male and (**b**, **d**, **f**) female Nx and IHx hippocampus at postnatal day (P) 30 ($n = 6$/group; biological replicates). **a**, **b** Heatmap of % fatty acids from total fatty acids z-scores. Content of (**c**, **d**) total and (**e**, **f**) ≥20 carbon saturated, ω-9, ω-5-7, ω-6 and ω-3 fatty acids. Data points (circles/triangles) represent ug of FA/total lipid and bars represent % of total fatty acids. Black * is significantly different as ug of FA/total lipid and grey * as % of total fatty acids. For (**c**–**f**), data are presented as mean ± SEM. Statistical analysis for (**a**–**f**) by unpaired Mann-Whitney 2-tailed test; *$p < 0.05$ Nx vs IHx (For (**c**) ω-9/Total FA (%) $p = 0.0022$, ω-6/Total FA (%) $p = 0.0043$, for (**e**) ≥20 C Saturated/Total FA(%) $p = 0.0043$, ≥20 C ω-9/Total FA (%) $p = 0.0022$, ≥20 C ω-6/Total FA (%) $p = 0.0043$, and for (**f**) ≥20 C Saturated/Total FA(%) $p = 0.0411$. FA, fatty acids, Sat, saturated. Source data are provided as a Source Data file.

https://doi.org/10.1038/s41467-025-67542-6

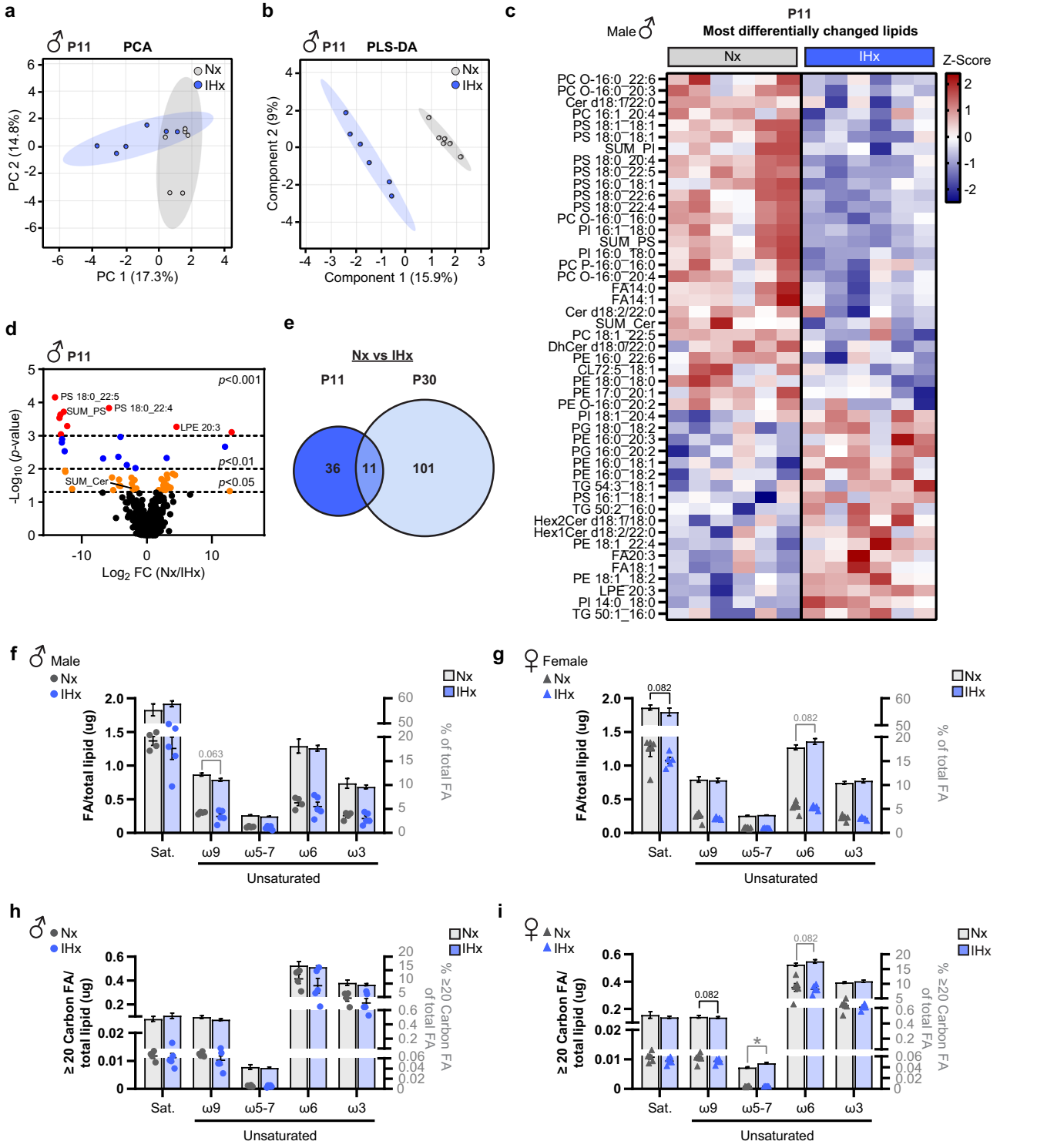

preterm compared to term infants are similar to the results from the IHx murine experiments at P11. Taken together, our data indicate that changes in brain lipid composition begin to emerge in IHx-injured mice as early as P11 but become prominent at a later age.

Since the brain depends on a continuous supply of substrates for metabolism and de novo lipid synthesis, we first sought to determine whether the observed dysregulated lipid metabolism is due to an altered supply of nutrients following IHx. The developing brain relies on glucose extensively for local de novo synthesis of fatty acids and as a substrate for energy[22,24]. In contrast to the adult brain, the developing brain uses alternative substrates such as ketones and lactate for energy and metabolism, while fatty acids imported from the circulation are used for the synthesis of complex lipids in the brain[28,29]. No hypoglycemia was observed in the IHx group (Supplementary Fig. 3a). Using ^{3}H-2-Deoxy-D-glucose (2-DG), we determined that glucose uptake in the hippocampus was comparable between the Nx and IHx males (Supplementary Fig. 3b). Of note, only females at P11 in the IHx group showed lower levels of blood glucose (Supplementary Fig. 3a) and decreased tracer uptake in the hippocampus at P11 and P30 (Supplementary Fig. 3b). Brain glucose 2-DG uptake was not correlated with plasma 2-DG (Supplementary Fig. 3b-d). As expected, systemic lactate levels were increased in the IHx group at P11 only (Supplementary

Fig. 3 | IHx alters brain lipid composition as early as P11. a–d Lipid profiling using liquid chromatography with tandem mass spectrometry (LC-MS/MS) in male Nx and IHx hippocampus at postnatal day (P) 11 ($n = 6$/group; biological replicates). **a** Principal component analysis (PCA) and (**b**) partial least-squares discriminate analysis (PLS-DA) score plots of lipid profiles comparing Nx and IHx. In (**a**, **b**), elliptical patterns represent 95% confidence intervals. **c** Heatmap of the 47 differentially changed lipids between Nx and IHx groups (Distanced measure: Euclidean; clustering algorithm: Ward). **d** Volcano plot depicting changes in lipids species between Nx and IHx groups. Black dots: $p > 0.05$; yellow dots: $0.05 > p > 0.01$; blue dots: $0.01 > p > 0.001$; red dots: $p < 0.001$. The x-axis is log2 (fold change; FC) and the y-axis is −log10 (p-value based on 2-tailed unpaired t-test performed by MetaboAnalyst without adjustments for multiple comparisons). **e** Venn diagram showing overlap of the total number of significantly changed lipids in Nx vs IHx P11 mice compared to Nx vs IHx P30 mice. **f–i** Total fatty acids quantified by gas chromatography with tandem mass spectrometry (GC/MS) in (**f**, **h**) male and (**g**, **i**) female Nx and IHx hippocampus at P11 (male: Nx $n = 4$, IHx $n = 5$; female Nx $n = 6$, IHx $n = 5$; biological replicates). Content of (**f**, **g**) total and (**h**, **i**) ≥20 carbon saturated, ω-9, ω-5-7, ω-6 and ω-3 fatty acids. Data points (circles/triangles) represent ug of FA/total lipid and bars represent % of total fatty acids. Black * is significantly different as ug of FA/total lipid and grey * as % of total fatty acids. For (**f**–**i**), data are presented as mean ± SEM. Statistical analysis by unpaired Mann-Whitney 2-tailed test; *$p < 0.05$ Nx vs IHx (For (**i**) ≥20 C ω-5-7/Total FA (%) $p = 0.0087$). N.d not detected, Cer ceramide, CL cardiolipin, DhCer dihydroceramide, FA fatty acids, HexCer hexosylceramide, LPE lysophosphatidylethanolamine, PC phosphatidylcholine, PE phosphatidylethanolamine, PG phosphatidylglycerol, PI phosphatidylinositol, PS phosphatidylserine, Sat saturated, TG triacylglycerol. Source data are provided as a Source Data file.

Fig. 3e). Circulating levels of non-esterified fatty acids (NEFA) were significantly decreased in both sexes at P22 in the IHx-treated group, which, interestingly, occurred immediately after weaning (Supplementary Fig. 3f). NEFA metabolism generates ketones and acylcarnitines (ACs), which are intermediates of fatty acid oxidation. Indeed, the plasma levels of the ketone body β-hydroxybutyrate (βHB) and of acylcarnitines (ACs) were increased at P11 and P17 compared to Nx controls (Supplementary Figs. 3g, 4a–d, Supplementary Table 8). To determine whether blood AC levels reflect brain ACs, we measured ACs in the hippocampus and the results showed that total ACs were increased only at P11 indicating that fatty acids were mobilized for subsequent generation of acetyl-CoA (Supplementary Fig. 4e–h, Supplementary Table 9). Furthermore, there was no deficiency of carnitine in the hippocampus of the IHx-injured group (Supplementary Fig. 4e). In fact, the level of free carnitine in the brain was increased, thus being readily available to facilitate fatty acid entry into the mitochondria via the carnitine shuttle for subsequent β-oxidation. Altogether, these data show that dysregulated brain lipid homeostasis is not the result of a limited supply of nutrients.

These substrates provide the mitochondrial generated carbons for subsequent de novo lipid synthesis. Therefore, we question whether changes in mitochondrial content could compromise the brain's ability to utilize these substrates after the injury. We quantified mitochondrial content by digital PCR and our results revealed that at P11 the ratio of mitochondrial DNA (mtDNA) to nuclear DNA (gDNA) was lower following IHx but recovered by P30 (Fig. 4a, Supplementary Fig. 5a). Since we observed the changes in mitochondrial content immediately after IHx, we performed an unbiased proteomics analysis of the hippocampus to better understand the changes that occur at this age (P11) and to identify proteins and pathways that may be responsible for abnormal lipid composition following IHx.

IHx affects the expression of lipid metabolism genes and proteins

Immediately after IHx (P11), pathway analysis of the proteomics revealed that the most significantly downregulated proteins belong to the metabolism pathway (Fig. 4b, c, Supplementary Fig. 5b–e). Within the metabolism pathway, we found that metabolism of lipids was one of the top three most downregulated pathways (Fig. 4b, Supplementary Fig. 5b, d). Because lipid-related proteins were downregulated in these pathways at P11, we assessed the temporal expression of genes crucial for lipid metabolism, specifically genes involved in fatty acid synthesis and oxidation, lipid regulation, and cholesterol and ketone metabolism in the hippocampus (Fig. 4d, e, Supplementary Fig. 6). The mRNA data showed that IHx resulted in a transient decrease of genes involved in lipid metabolism. Specifically, following IHx, the expression of genes responsible for fatty acid oxidation *(Cpt2)*, synthesis of long-chain fatty acids and cholesterol (*Scd2, Elovl6, Hmgcr*), and lipid regulators (*Acc1*) were decreased at P11, P17, and P22 (Fig. 4d, e, Supplementary Fig. 6a–d). However, they not only recovered by P30, but some of these genes were upregulated at this age (*Srebp2, Hmgcr*) (Supplementary Fig. 6c, d). Similarly, the expression of *Fasn* – an enzyme system responsible for de novo synthesis of primarily palmitate (C16:0) - was downregulated at P11 and subsequently upregulated at P30 (Fig. 4d and Supplementary Fig. 6a). *Elovl5*, which is essential for the elongation of ω-3 and ω-6 fatty acids, was not changed (Fig. 4d and Supplementary Fig. 6a). These results showed that IHx downregulates the expression of lipid metabolism related genes as early at P11, however, these changes were transient and recovered by P30. Moreover, it is important to point out that these genes are subject to post-transcriptional, post-translational, and allosteric regulation[23,30]. While the unbiased proteomics and gene expression analyses highlight interesting findings, they do not assess function. Therefore, in addition to gene expression and proteomics analysis, we then sought to determine the functional alterations by which neonatal intermittent hypoxia results in long-term changes in brain lipid composition.

IHx increases fatty acid oxidation and alters lipid composition at P17

We first tested the dependency of the injured brain on different substrates as fuel for energy production by performing the Seahorse XF Mito Fuel Flex test in single-cell suspensions from the hippocampus (Fig. 5a). We found that the injured brain had a decreased dependency on glucose for fuel at P11 (Fig. 5a). There were no differences observed in mitochondrial glutamine dependency at any of the ages studied (P11, P17, P30) (Fig. 5a). Interestingly, the IHx-injured group had a significant increase in dependency on fatty acids as a fuel at P11, and this persisted up to P17, six days after recovery from IHx (Fig. 5a). At P30, there was a significant decrease in fatty acids dependency in IHx-injured mice compared to Nx (Fig. 5a). To validate our findings, we measured the oxidation of [^{14}C]-substrates to $^{14}CO_2$ ex-vivo in microdissected hippocampi in both groups (Supplementary Fig. 7a). [U-^{14}C]-glucose oxidation was increased only at P11 (Supplementary Fig. 7b) whereas the fatty acid [1-^{14}C]-oleic acid (C18:1) oxidation was increased at P11 and P17 (Fig. 5b, Supplementary Fig. 7c). There were no differences in ^{14}C-acid soluble metabolites (ASM) generated by [1-^{14}C]-oleic acid oxidation (Supplementary Fig. 7d). Because the oxidation of fatty acids remained high during the subsequent 6 days after the injury, we sought to determine whether the developing brain had increased circulating fatty acid uptake into the brain at P17 (Supplementary Fig. 7e–g). Thus, we measured the uptake of ^{3}H-2-bromopalmitate, an analogue of the fatty acid palmitate that cannot be β-oxidized and showed a significant increase in IHx-injured mice (Supplementary Fig. 7e–g). Furthermore, at P17, we measured the oxidation of other alternative substrates. The oxidation of [U-^{14}C]-glutamine, [3-^{14}C]-βHB, and [U-^{14}C]-lactate did not change at P17 in IHx-injured mice compared to Nx controls (Supplementary Fig. 7h–j). Taken together, these data show that immediately after intermittent hypoxia (P11- acute period) and during the recovery period under normoxic conditions (P17 -

https://doi.org/10.1038/s41467-025-67542-6

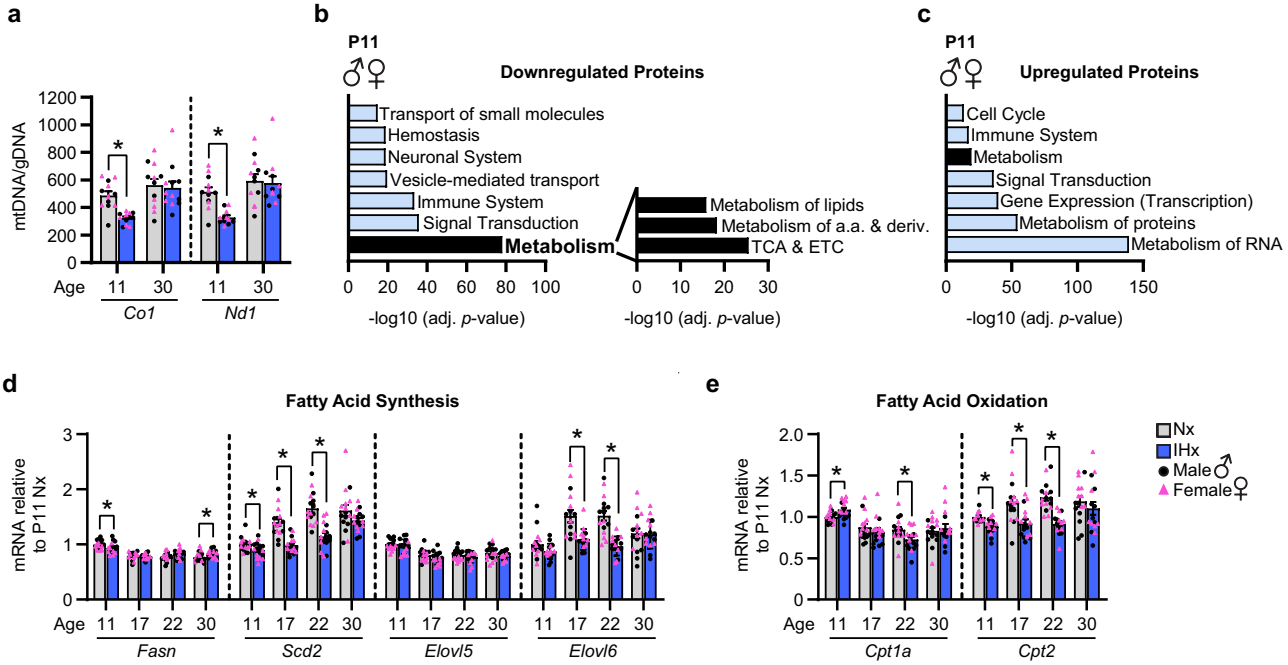

Fig. 4 | IHx affects the expression of genes and proteins involved in lipid metabolism. a Digital PCR was performed to determine mitochondrial content by normalizing mitochondrial DNA copy numbers (*Co1* and *Nd1*) to nuclear DNA (*H19*) in hippocampus from Nx and IHx mice at postnatal day (P) 11 and P30 ($n = 6$/sex/age/group; biological replicates). **b**, **c** Unbiased proteomics analysis of P11 hippocampus after IHx by ANOVA method without adjustments for multiple comparisons; $n = 4$/sex/group; biological replicates). Pathway analysis of differentially expressed proteins (p-value < 0.05) between Nx and IHx hippocampus was performed using g:Profiler (https://biit.cs.ut.ee/gprofiler/gost). g:SCS was selected as statistical threshold and p-value < 0.05 as the significance threshold. The (**b**) downregulated and (**c**) upregulated proteins from IHx hippocampus compared to Nx were analyzed through g:Profiler and the pathways from REACTOME were selected. The top 7 significant pathways ($p < 0.05$) belonging to the first hierarchical level were plotted. For the metabolism pathway within the (**b**) downregulated proteins, the top significant pathways belonging to the second hierarchical level were plotted. (-log10 (p-adjusted value)). **d**, **e** mRNA abundance of genes involved in fatty acid (**d**) synthesis and (**e**) oxidation in hippocampus from Nx and IHx mice, expressed as relative to P11 Nx ($n = 8$/sex/age/group; biological replicates). For (**a**, **d**, **e**) data are presented as mean ± SEM. Statistical analysis for (**a**, **d**, **e**) by unpaired Mann-Whitney 2-tailed test; *$p < 0.05$. Nx vs IHx within the same age (For (**a**) P11 *Co1* $p = 0.0001$, P11 *Nd1* $p = 0.0003$, for (**d**) *Fasn*: P11 $p = 0.0468$, P30 $p = 0.0234$, *Scd2*: P11 $p = 0.0468$, P17 and P22 $p = <0.0001$, *Elovl6*: P17 $p = 0.0007$ and P22 $p = <0.0001$, and for (**e**) *Cpt1a*: P11 $p = 0.0152$, P22 $p = 0.0426$, *Cpt2*: P11 $p = 0.0003$, P17 $p = 0.0039$, P22 $p = <0.0001$). Males black circles, Females pink triangles. *Co1* cytochrome c oxidase I, *Nd1* NADH dehydrogenase 1, mtDNA mitochondrial DNA, gDNA nuclear DNA, a.a amino acids, deriv. derivatives, ETC electron transport chain, TCA tricarboxylic acid cycle, *Fasn* Fatty acid synthase, *Scd2* stearoyl-CoA desaturase 2, *Elovl5* elongation of very long chain fatty acid protein 5, *Elovl6* elongation of very long chain fatty acid protein 6, *Cpt1a* carnitine palmitoyltransferase 1 A, *Cpt2* carnitine palmitoyltransferase 2. Source data are provided as a Source Data file.

6 days after IHx), the developing brain upregulates long-chain fatty acid oxidation to fuel and support oxidative metabolism.

Previous studies showed that neural progenitor cells and astrocytes express the enzymatic machinery for fatty acid oxidation[3,4,31]. In this study we used a conditional knockout mouse of carnitine palmitoyltransferase-2 (CPT2), an obligatory enzyme for mitochondrial long-chain fatty acid β-oxidation (Supplementary Fig. 7k)[3]. We determined that [1-^{14}C]-oleic acid oxidation was significantly decreased after IHx in both pan-brain (Nestin-Cre; CPT2$^{B-/-}$) and astrocyte-specific (Gfap-Cre; CPT2$^{G-/-}$) knockout mice compared to IHx-injured wild-type mice (Fig. 5c, Supplementary Fig. 7l, m). These results indicate that after IHx, astrocytes are the primary brain cells that oxidize fatty acids.

Since long-chain fatty acids were being extensively oxidized during the recovery from IHx up to P17, we analyzed the fatty acid profile of P17 hippocampus to determine if the fatty acid composition was also affected at this time point. Compared to Nx control, P17 IHx-injured mice displayed changes in total fatty acid composition similar to P30 IHx-injured mice (Figs. 2a, b, 5d, e, Supplementary Tables 2, 3, 10, 11). Notably, IHx had a significant, or trending, lower percent of total brain ω−9 fatty acids in both sexes (Fig. 5f, g). These ω−9 fatty acids are synthesized extensively in the brain and accumulate during development. Specifically, our analysis revealed a reduction in saturated and ω−9 fatty acids composed of ≥20-carbons in IHx-injured mice of both sexes compared to Nx (Fig. 5h, i). These long and VLCFA, are exclusively synthesized de novo in the brain[32]. In addition, oleic acid (C18:1n−9) was decreased in the IHx-injured mice (male, $p = 0.082$, female $p < 0.05$) (Fig. 5d, e, Supplementary Tables 10, 11). In contrast to decreased levels of ≥20 carbon-long fatty acids, IHx resulted in significant, or trending, increases in the percent of C14:0, C16:1(n-7), 16:1(n-9), C18:3(n-6), and C20:3(n-7) fatty acids in both male and female pups (Fig. 5d, e, Supplementary Tables 10, 11). Furthermore, in males we observed increased levels of the medium-chain fatty acids (C10:0, C12:0, C10:1) as well as C18:2(n−6) compared to Nx controls (Fig. 5d, Supplementary Table 10). Altogether, these data suggest that IHx leads to reduced levels of saturated and unsaturated ω−9 ≥ 20 carbon-long fatty acids in the hippocampus as early as P17, resulting in a shift in total fatty acid composition.

Next, we aimed to further characterize in situ these lipid fatty acid profile changes following IHx at P17. Using non-targeted matrix-assisted laser desorption/ionization mass spectrometry imaging (MALDI-MSI), we identified several ions corresponding to lipid species containing medium or long-chain saturated and monounsaturated fatty acids that increased after IHx across multiple brain regions (PC(30:0) – *m/z* 744.4929 [M + K]$^+$ and PC(32:1) – *m/z* 770.5080 [M + K]$^+$) (Fig. 6a). Conversely, ions corresponding to lipids containing ≥18 carbons saturated and monounsaturated fatty acids were decreased after IHx (PC(36:1) – *m/z* 826.5701 [M + K]$^+$ and SM(36:1;O2) – *m/z* 769.5609

https://doi.org/10.1038/s41467-025-67542-6

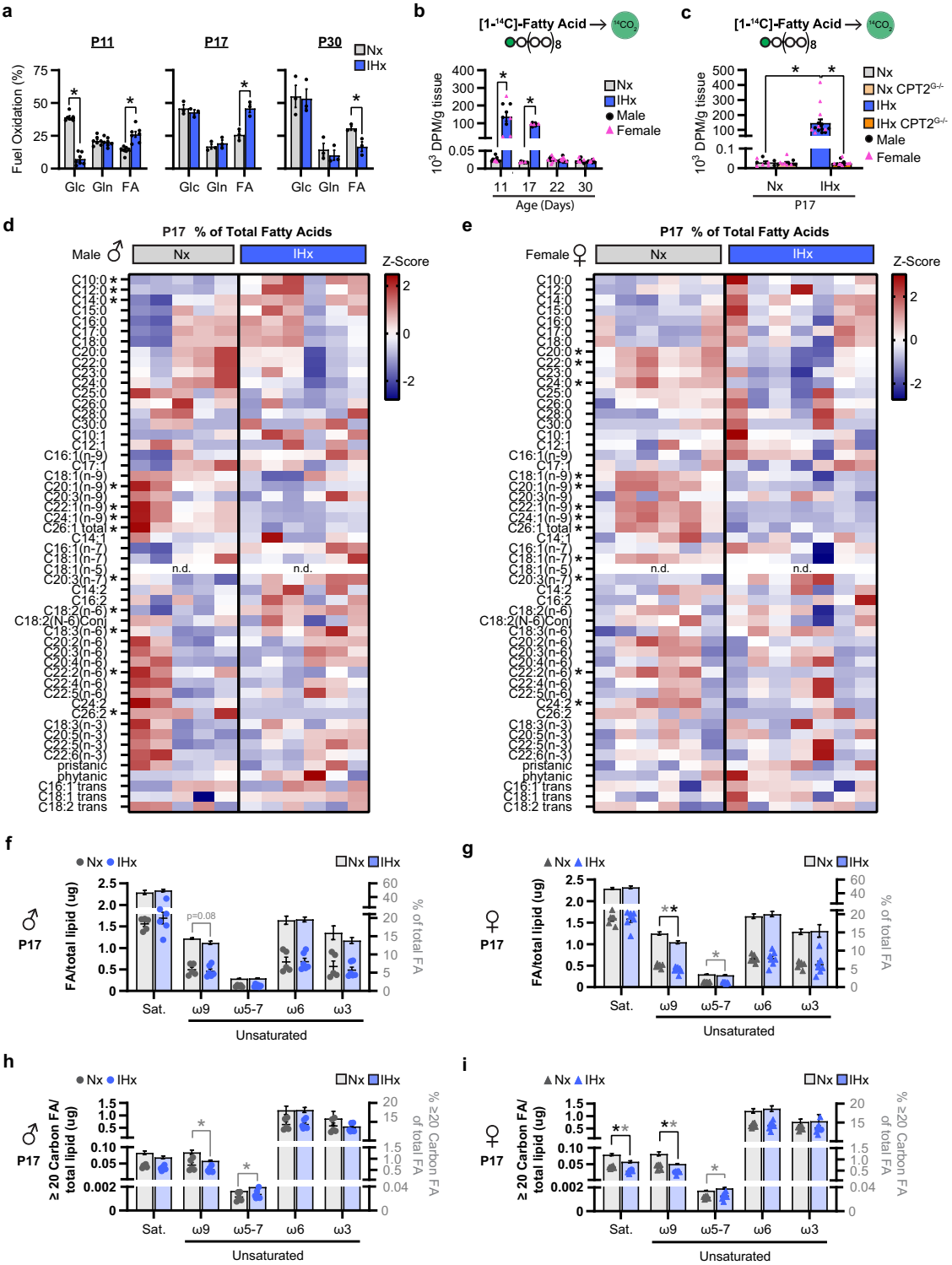

$[M + K]^+$ (Fig. 6b). Quantification of ion intensities in the hippocampus showed statistically significant changes in these lipid species (Fig. 6c, d). Furthermore, lipid mapping using MALDI-MSI also enabled us to detect subregional differences. For example, PC(32:1) is highly enriched in the dentate gyrus (white arrows) while SM(36:1;O2) in the CA3 (pink arrow) (Fig. 6a, b). These results corroborate the total lipid fatty acid profile at P17 (Fig. 5d) and provide additional evidence of changes observed in the lipidomic profile at P30 (Fig. 1e–h). Together, these data demonstrate that IHx results in hippocampal region-specific lipid changes and that these lipid changes are congruent with the lipid fatty acid chain composition.

To get a more detailed understanding of the specific lipid changes that occur at P17, six days after recovery from IHx, we performed lipidomic analysis (Fig. 6e–h, Supplementary Table 12). PCA showed a partial overlap between the Nx and IHx groups, whereas the PLS-DA demonstrated distinct separation suggesting that the lipid profile vary between groups (Fig. 6e, f). Indeed, by P17 there were more lipid changes observed compared to the IHx P11 group (47 lipids at P11 vs 76 lipids at P17). Among the top 50 most differentially changed lipids, several phosphatidylethanolamine (PE) lipid species containing 18–20 carbon-long saturated and monounsaturated fatty acids were decreased after IHx (Fig. 6g, Supplementary Table 12). The majority of

Fig. 5 | IHx increases fatty acid oxidation and alters fatty acid composition at P17. a SeahorseXF Mito Fuel Flex test performed in single cell suspensions from Nx and IHx hippocampus at postnatal day (P) 11, P17, and P30 (P11 $n = 7$/group; P17 and P30 $n = 3$/group; biological replicates). Glc glucose, Gln glutamine, FA fatty acid. **b** Ex-vivo hippocampal [1-^{14}C]-oleic fatty acid oxidation to $^{14}CO_2$ in Nx and IHx mice (P11 $n = 9$/group; P17 $n = 8$/group; P22 Nx $n = 14$, IHx $n = 13$; P30 Nx $n = 8$, IHx $n = 9$; biological replicates). **c** Ex-vivo hippocampal [1-^{14}C]-oleic fatty acid oxidation to $^{14}CO_2$ in control and CPT2 astrocyte-specific knockout ($CPT2^{G-/-}$) P17 mice that underwent Nx or IHx (control Nx $n = 9$, IHx $n = 15$; $CPT2^{G-/-}$ Nx $n = 11$, IHx $n = 16$; biological replicates). **d-i** Total fatty acids quantified by gas chromatography with tandem mass spectrometry (GC/MS) in (**d**, **f**, **h**) male and (**e**, **g**, **i**) female Nx and IHx hippocampus at P17 (Male: Nx $n = 5$, IHx $n = 6$; female: Nx $n = 6$, IHx $n = 7$; biological replicates). **d**, **e** Data are presented as a heatmap of % fatty acids from total fatty acids z-scores. Content of (**f**, **g**) total and (**h**, **i**) ≥20 carbon-long saturated, ω-9, ω-5-7, ω-6 and ω-3 fatty acids. For (**f**–**i**) data points (circles/triangles) represent ug of FA/total lipid and bars represent % of total fatty acids. Black * is significantly different as ug of FA/total lipid and grey * as % of total fatty acids. (**a**–**c**, **f**–**i**) data are presented as mean ± SEM. Statistical analysis for (**a**) by 2-tailed unpaired student's t-test, for (**b**–**i**) by unpaired Mann-Whitney 2-tailed test; *$p < 0.05$ Nx vs IHx within the same age (For (**a**) P11 Glc $p = <0.000001$, FA $p = 0.0004$, P17 FA $p = 0.0075$, P30 FA $p = 0.0241$, for (**b**) P11 $p = 4.10\times10^{-5}$, P17 $p = 0.0002$, for (**c**) Nx control vs IHx control $p = <0.0001$, IHx control vs IHx $CPT2^{G-/-}$ $p = <0.0001$, for (**g**) ω-9/Total Lipid (ug) $p = 0.0140$, ω-9/Total FA (%) $p = 0.0012$, ω-5-7/Total FA (%) $p = 0.0350$, for (**h**) ≥20 C ω-9/Total FA (%) $p = 0.0043$, ≥20 C ω-5-7/Total FA (%) $p = 0.0303$, and for (**i**) ≥20 C Saturated/Total Lipid (ug) $p = 0.0012$, ≥20 C Saturated/Total FA (%) $p = 0.0023$, ≥20 C ω-9/Total Lipid (ug) $p = 0.0012$, ≥20 C ω-9/Total FA (%) $p = 0.0012$, ≥20 C ω-5-7/Total FA (%) $p = 0.0082$). FA fatty acids, DPM disintegrating parts per million, CPT2 carnitine palmitoyltransferase 2, n.d. not detected, Sat saturated. Source data are provided as a Source Data file.

the lipids that were increased belonged to the sphingolipids lipid class, which included hexoceramides (Hex1Cer), dihexoceramides (Hex2-Cer), sphingomyelin, dihydroceramides (DhCer), and ceramides (Fig. 6g, Supplementary Table 12). Volcano plot analysis revealed that there were many more significantly changed lipids displaying a large increase after IHx (Log2-fold change >15) compared to those that were decreased (14 increased vs 2 decreased) (Fig. 6h). Together these data suggest that IHx affects the developmental lipid remodeling occurring in the hippocampus at P17.

The next critical transition of development is switching from a lipid-rich diet (suckling) to consuming a carbohydrate-rich diet. Hence, we determined the lipid composition of the hippocampus at P22, one day after pups weaning (Supplementary Fig. 8a–d, Supplementary Table 13). While PCA resulted in overlapping groups, PLS-DA clearly differentiated the Nx and IHx groups suggesting that the lipid profile continued to differ at P22 (Supplementary Fig. 8a, b). Hierarchical clustering and volcano plot analysis revealed increase levels of several triacylglyceride species (Supplementary Fig. 8c, d, Supplementary Table 13). Moreover, ceramides were still increased at this time point (Supplementary Fig. 8c, Supplementary Table 13). In addition to analyzing the lipid classes, we measured total lipid fatty acids (Supplementary Fig. 8e-g, Supplementary Table 14,15). Interestingly, in males, while total saturated fatty acids were comparable between Nx and IHx, the levels of palmitate (C16:0) – the primary product of de novo lipogenesis – was increased in the IHx group (Supplementary Fig. 8e,f, Supplementary Table 14). In females, palmitate levels did not differ between Nx and IHx groups (Supplementary Fig. 8e, Supplementary Table 15). The percent of total saturated and ω-9 fatty acids composed of ≥20-carbons showed a trend towards a decrease only in the IHx-injured female mice compared to Nx (Supplementary Fig. 8g). Altogether, our data show that brain palmitate levels were not compromised despite switching to a carbohydrate-rich diet due to weaning (P21) and subsequent decrease in circulating NEFA (P22) (Supplementary Fig. 3f). These results corroborate our findings that de novo lipogenesis is similar between Nx and IHx groups (Supplementary Fig. 1f).

Acetate as an alternative substrate to reduce fatty acid oxidation

The mitochondrial β-oxidation of fatty acids generates acetyl-CoA which enters the tricarboxylic acid (TCA) cycle and enables the generation of adenosine triphosphate (ATP)[33]. Acetyl-CoA is a key metabolite that serves as a building block for the synthesis of de novo fatty acids, proteins, and amino acids[33]. Hence, maintaining the pool of acetyl-CoA is critical for cellular metabolism. We reasoned that supplementing the media with a higher concentration of glucose, a substrate that can be metabolized to yield acetyl-CoA, will spare fatty acids from oxidation in the injured brain. However, high glucose concentrations (25 mM) in the media did not affect [1-^{14}C]-oleic acid oxidation compared to 5 mM glucose at P17 after IHx (Fig. 7a, Supplementary Fig. 9a). Thus, we next measured the oxidation of fatty acids in the presence of acetate, a substrate that can be directly converted to acetyl-CoA. Media supplementation with 2 mM acetate resulted in an 86% and 93% reduction in [1-^{14}C]-oleic acid oxidation at P11 and P17, respectively, compared to IHx-injured hippocampus without acetate supplementation (Fig. 7a, Supplementary Fig. 9a,b). Moreover, [1,2-^{14}C]-acetate oxidation increased after IHx and was not affected by the presence of different oleic acid concentrations (Fig. 7b, Supplementary Fig. 9c). These results indicate that acetate supplants fatty acids for oxidation in the IHx-injured hippocampus.

We next sought to determine whether in vivo acetate administration will spare brain fatty acids from oxidation after IHx, and therefore improve neurologic outcome. Glycerol-triacetate (Triacetin) is an FDA-approved compound that consists of three acetate moieties esterified to a glycerol backbone (Fig. 7c)[34]. Glycerol-triacetate is readily absorbed in the gut, crosses the blood-brain barrier, and has demonstrated non-toxic effects[34]. Hence, we chose to administer glycerol-triacetate to supply acetate as an alternative fuel for brain metabolism. Glycerol-triacetate was administered to pups by oral gavage (5 mg/g body weight) daily from P11 to P17 (Fig. 7c). In the IHx-injured group, treatment with glycerol-triacetate reduced hippocampal [1-^{14}C]-oleic acid oxidation by 71% at P17 compared to glycerol (vehicle) (Fig. 7d, Supplementary Fig. 9d, e).

To assess whether treatment with glycerol-triacetate can promote neurological recovery after neonatal injury, we performed behavioral testing at P30 following IHx. Using mice treated with glycerol-triacetate (treatment) or glycerol (vehicle) from P11 to P17, we performed the novel object recognition (NOR) test at P30 (Fig. 7e and Supplementary Fig. 9f). IHx-mice treated with glycerol-triacetate showed a significantly increased recognition index in the NOR compared to controls, suggesting an improvement in recognition memory (Fig. 7e and Supplementary Fig. 9f). Together, these data show that treatment with glycerol-triacetate spares fatty acids from mitochondrial β-oxidation and improves neurologic outcome.

Treatment with glycerol-triacetate did not restore body and brain weight in IHx-injured mice by P30 and the percent of total lipids per mg of hippocampus remained the same as the Nx controls (Fig. 7f, g and Supplementary Fig. 9g–i). However, total lipid fatty acid analysis showed that treatment with glycerol-triacetate after IHx restored total lipid fatty acid composition (Fig. 7h-l and Supplementary Fig. 9j–m, Supplementary Tables 16, 17). Specifically, the decrease percent of total ω−9 fatty acids in IHx mice was recovered after glycerol-triacetate treatment in both sexes (Fig. 7i, j). The levels of oleic acid (18:1n−9) that we previously demonstrated to be decreased in the P30 IHx males (Fig. 2a, Supplementary Table 2), were similarly decreased in the IHx-glycerol treated males and restored by glycerol-triacetate treatment (Fig. 7h, Supplementary Table 16). Importantly, glycerol-triacetate treatment prevented the IHx-induced low levels of ≥20-carbon

https://doi.org/10.1038/s41467-025-67542-6

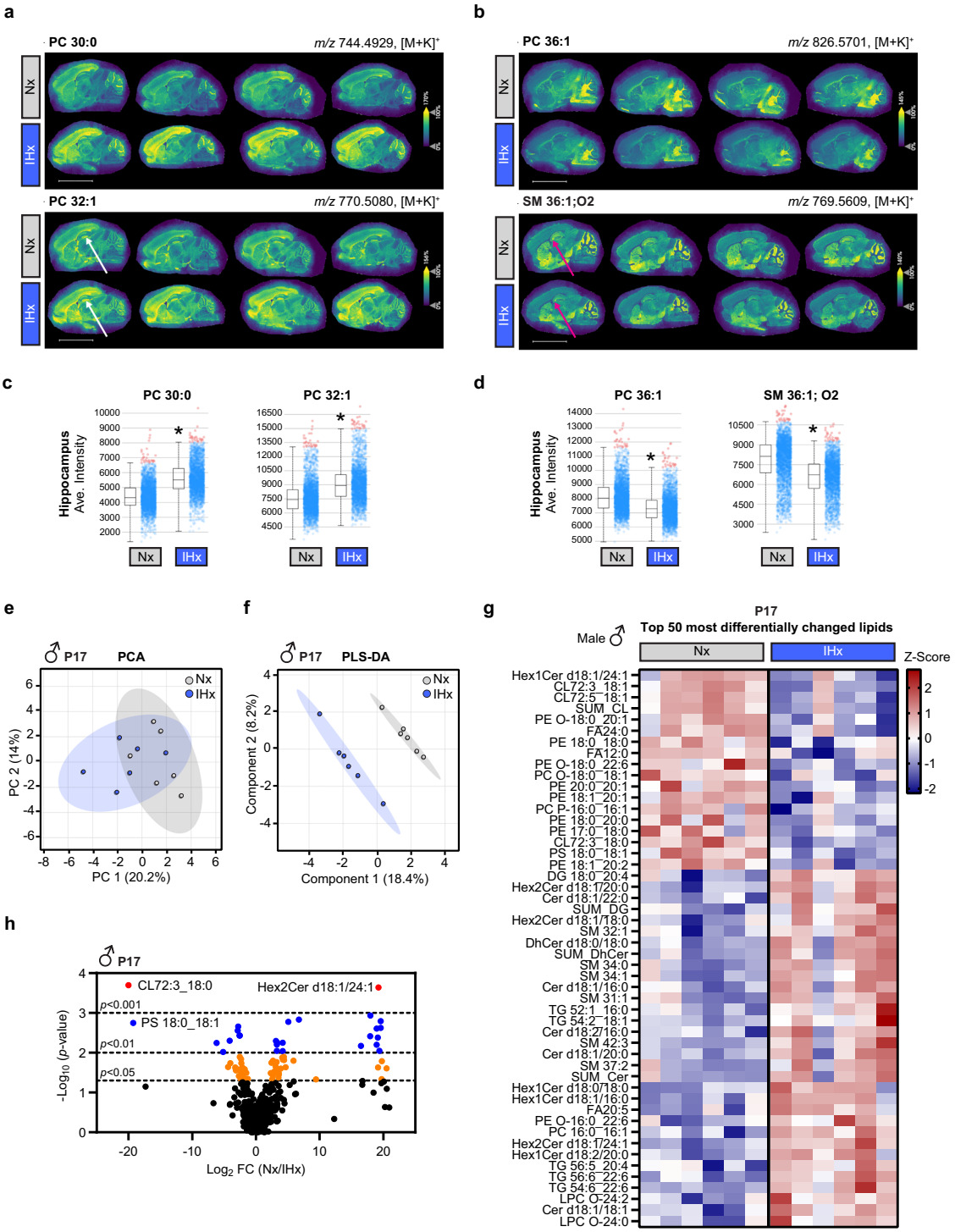

saturated and ω−9 fatty acids (Fig. 7h, k, l). The increase levels of C16:0 in IHx-injured males was reversed to normoxia levels after glycerol-triacetate administration (Fig. 7h, Supplementary Table 16). Together, these data show that treatment with glycerol-triacetate restores the levels of ≥20 carbon-long saturated and ω-9 fatty acids in the hippocampus of IHx-injured mice.

In conclusion, our results reveal that brain fatty acid oxidation, which is negligible in the developing brain, is significantly upregulated following neonatal brain injury from IHx. This shift towards brain fatty acid oxidation leads to decreased levels of ≥20 carbon-long and very-long chain saturated and ω-9 fatty acids, which are synthesized in the brain de novo. Ultimately, this change in fatty acid metabolism disrupts highly orchestrated lipid-rich brain development and maturation and leads to sustained behavioral deficits. An alternative fuel - acetate - can spare fatty acids from oxidation following neonatal brain injury. Treatment with glycerol-triacetate, an FDA-approved compound that provides acetate and can be administered by enteral route, may rescue brain lipid metabolism during a critical period of brain development and prevent cognitive delays associated with intermittent hypoxemia in infants born EPT.

Discussion

Although it is well recognized that neonatal brain injury affects brain development, the extent to which it alters brain lipid composition

Fig. 6 | IHx induces global changes in brain lipid composition. a–d In-situ MALDI-MSI analysis of brain lipids in postnatal day (P) 17 Nx and IHx male mice ($n = 4$/group; biological replicates; experiment was performed one time). **a**, **b** Distribution of lipids containing (**a**) medium- or long-chain saturated and monounsaturated fatty acids and (**b**) lipids containing ≥18 carbons saturated and monounsaturated fatty acids. Yellow signifies the highest intensity and blue the lowest of each *m/z*. White arrows in (**a**) indicate the dentate gyrus of the hippocampus and the pink arrows in (**b**) indicate the CA3 region. **c**, **d** Box plot of the intensity of total ion signals in the hippocampal area. Box plots show the median (center line), 25–75% range (lower and upper boundaries of box) and outliers (whiskers). Statistical analysis by 2-tailed paired t-test; $^{*}p < 0.05$ (For (**c**) PC(30:0) $p = 0.0002$, PC(32:1) $p = 0.0006$ and for (**d**) PC(36:1) $p = 0.0005$, SM(36:1;O2) $p = 0.0003$). **e-h** Lipid profiling using liquid chromatography with tandem mass spectrometry (LC-MS/MS) in male Nx and IHx hippocampus at P17 ($n = 6$/group; biological replicates). **e** Principal component analysis (PCA) and (**f**) partial least-squares discriminate analysis (PLS-DA) score plots of lipid profiles comparing Nx and IHx. In (**e**, **f**), elliptical patterns represent 95% confidence intervals. **g** Heatmap of the top 50 differentially changed lipids between Nx and IHx groups (Distanced measure: Euclidean; clustering algorithm: Ward). **h** Volcano plot depicting changes in lipids species between Nx and IHx groups. Black dots: $p > 0.05$; yellow dots: $0.05 > p > 0.01$; blue dots: $0.01 > p > 0.001$; red dots: $p < 0.001$. The x-axis is log2 (fold change; FC) and the y-axis is −log10 (*p*-value based on 2-tailed unpaired t-test performed by MetaboAnalyst without adjustments for multiple comparisons). $[M + K]^+$, potassium adduct of the molecular ion, *m/z* mass-to-charge ratio, Cer ceramide, CL cardiolipin, DhCer dihydroceramide, DG diacylglycerol, FA fatty acid, HexCer hexosylceramide, LPC lysophosphatidylcholine, PC phosphatidylcholine, PE phosphatidylethanolamine, PS phosphatidylserine, SM sphingomyelin, TG triacylglycerol. Source data are provided as a Source Data file.

acutely and during recovery has not been examined. This study provides crucial evidence that neonatal brain injury from intermittent hypoxemia results in an increase in fatty acid oxidation and extensive long-term changes in hippocampal lipid composition at age-equivalent to school-age children.

With advances in neonatal critical care, there is a growing population of children and young adults born extremely preterm (EPT; <28 weeks) who have persistent cognitive deficits that become increasingly apparent at school age[5,35,36]. Numerous human observational studies reported that children and adults with a history of prematurity display reduced volumes of the hippocampus, an area of the brain that is responsible for memory consolidation, spatial navigation, and learning[13,37,38]. Accumulated evidence have shown that neonatal brain injury affects brain growth and maturation processes such as myelination, synaptic formation, and dendritic arborization – processes highly dependent on a specific composition of lipids[14,39–42]. Based on our results, neonatal brain injury from intermittent hypoxemia significantly perturbed hippocampal lipid composition both acutely and during the subsequent period of brain development and maturation (P30). Specifically, we observed changes in sphingolipids and phospholipids, which are important for myelination and synaptic formation[43–45]. Since the brain heavily relies on fatty acids as essential building blocks of these complex lipids, and many of them are synthesized de novo in the brain, we performed a comprehensive characterization of total lipid fatty acids. Our data revealed that neonatal brain injury due to IHx causes a shift in the fatty acid profile, particularly by decreasing the levels of ≥20 carbon-long saturated and ω-9 fatty acids, which are synthesized de novo in the brain and are essential for neuronal development and function[32,46].

De novo synthesis of fatty acids occurs at high rates during development, and our total fatty acid analysis at different time points delineates the trajectory of brain fatty acid accretion during this critical period. Under normal conditions, palmitate, the most abundant fatty acid in the brain, has a higher percent of total fatty acid pool at P11 (~32%; 0.73 ug/ug of lipid) and subsequently decreases (P30 - ~24%; 1 ug/ug of lipid). In contrast, the percent of ≥20 carbon-long saturated fatty acids increase during development (P11 - ~0.5%; 0.011 ug/ug lipid vs P30 - ~2.4%; 0.11ug/ug lipid). Immediately after IHx (P11), and during early recovery (P17), the levels of palmitate in male hippocampus were comparable to the levels observed in Nx controls. These results were corroborated by total lipid fatty acid profile obtained from human samples, using hippocampal tissue from term and preterm newborns at similar corrected age (1-2 months). At later time points, following weaning (P22 and P30), the levels of palmitate significantly increase in the IHx group compared to Nx indicating increase de novo fatty acid synthesis. In contrast, females displayed palmitate levels equivalent to Nx hippocampus at all ages. Similarly, a prior study using adult mice reported sexual dimorphism in brain lipid composition and attributed these changes to differences in fatty acid uptake into the brain and expression of enzymes involved in fatty acid metabolism[47]. Indeed, we observed upregulation in the expression of fatty acid synthase (*Fasn*) at P30 in males but not in females after IHx. Taken together, these data suggest that the increase in hippocampal palmitate may indicate an endogenous attempt towards improved lipid profile during the recovery period from the IHx-injury.

Energy needs in the developing brain are high because it is a period of building, growth, and structural and functional maturation. However, the recovery process imposes additional energy demands. Here, we showed that these energy needs led to an increase in hippocampal fatty acid oxidation, and this dramatic increase was detected not only immediately after IHx but persisted for up to 6 days during the recovery period under normoxia conditions. Interestingly, fatty acid oxidation is age- and region-dependent and this process is negligible in the developing brain[4]. While fatty acid oxidation is not exclusive to a particular region, the hippocampus has a high capacity to oxidize fatty acids compared to cortex and midbrain[4]. In the developing brain, this upregulation in fatty acid metabolism disrupted highly orchestrated lipid-rich brain development and maturation and lead to hippocampal-dependent behavioral deficits (Novel object recognition and Y-maze). This is, interestingly, in contrast to the aging brain, which relies on fatty acid oxidation to sustain cognitive performance[31]. Likewise, other areas of the brain may be affected due to abnormal lipid composition, which can be delineated using spatial resolution techniques such as matrix-assisted laser desorption/ionization mass spectrometry imaging (MALDI-MSI).

In this study, the lipidomic profile was performed on microdissected hippocampus, thus, several cell types could be affected[48]. Our lipidomic profile has shown that at P30 (19 days post-IHx) several Hex1Cer and Hex2Cer species were both down- and up-regulated. Indeed, oligodendrocytes, which are abundant in the white matter and contain high levels of HexCer, can be affected in this model. Multiple levels of evidence have reported changes to astrocyte sphingolipid structure and metabolism in various neurodegenerative diseases[49–51]. Specifically, astrocyte production of cerebrosides (HexCer) as precursors to gangliosides supports healthy neurite outgrowth, regulates neuroinflammation, and stabilize neuron-glia interactions[52,53]. Furthermore, using genetic approaches we have shown that fatty acid oxidation is carried out specifically by astrocytes following IHx, which is consistent with a recent report in the adult brain[31].

It is generally accepted that increased protein expression is associated with increased function. Our proteomic data at P11, a time point at which fatty acid oxidation was most elevated, showed that the metabolism of lipids pathway was downregulated (Fig. 4b and Supplementary Fig. 5b, d). Interestingly, the expression of genes and/or proteins responsible for fatty acid oxidation (*Cpt2*, *Acadm*, and *Acadvl*) were downregulated in males but not in females at P11 (Supplementary Fig. 5b, d and 6b). Existing proteins might carry out activity very

https://doi.org/10.1038/s41467-025-67542-6

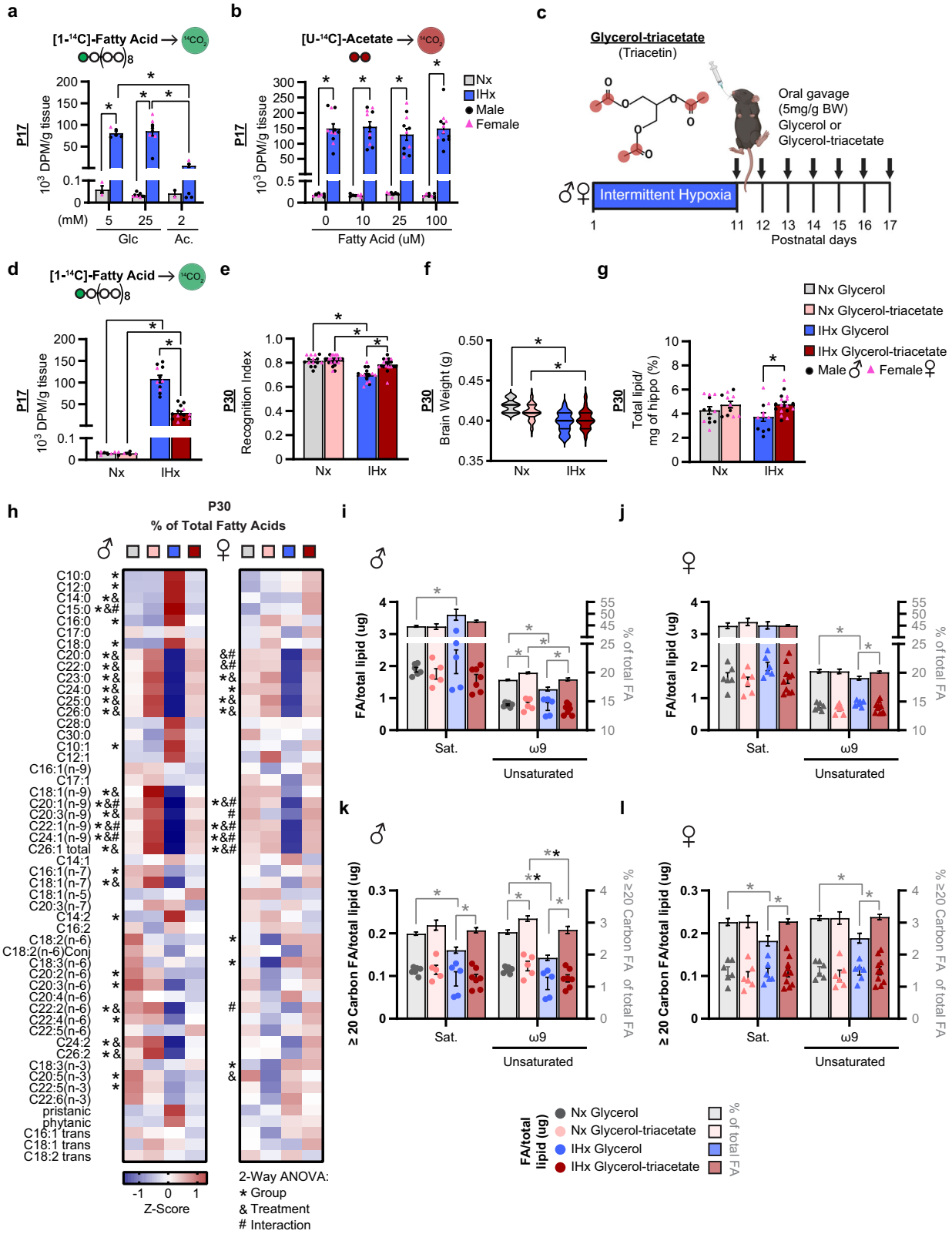

efficiently even at small levels, thus generating a negative feedback loop which results in post-translational changes, i.e., reduced transcription or increased degradation of mRNA. Likewise, decreased activity may trigger increase in mRNA expression and subsequent upregulation of protein expression. Our approach in this study was to comprehensively assess gene and protein expression as well as function since these might be discordant. This is in agreement with a recent report, albeit in another tissue (liver), which demonstrated discordance between the levels of mRNA, protein, and activity[54].

The brain relies on a constant supply of substrates for growth, development, and metabolism, which are delivered via systemic circulation. Glucose is the primary substrate for de novo lipogenesis in the developing brain[24]. Our results show that there was no hypoglycemia at any time point studied, albeit we observed some sex

Fig. 7 | Acetate serves as an alternative substrate to reduce fatty acids from being oxidized. a Ex-vivo postnatal day (P) 17 hippocampal [1-^{14}C]-oleic fatty acid oxidation to $^{14}CO_2$ in Nx and IHx mice in media containing 5 mM glucose, 25 mM glucose, or 2 mM acetate (Nx: 5 mM Glc $n = 3$, 25 mM Glc $n = 9$, 2 mM acetate, $n = 2$; IHx: 5 mM Glc $n = 5$, 25 mM Glc $n = 8$, 2 mM acetate $n = 5$; biological replicates). **b** Ex-vivo P17 hippocampal [1,2-^{14}C]-acetate oxidation to $^{14}CO_2$ in media containing 0, 10, 25, 100 uM cold oleic acid (Nx $n = 7$/group, IHx $n = 11$/group; biological replicates). **c** Glycerol-triacetate (Triacetin) chemical formula and schematic representation of the treatment plan. Red circles depict the acetate carbons within glycerol-triacetate. **d** Ex-vivo [1-^{14}C]-oleic fatty acid oxidation to $^{14}CO_2$ in hippocampus of Nx and IHx mice treated with glycerol or glycerol-triacetate (Nx glycerol $n = 7$, Nx glycerol-triacetate $n = 6$, IHx glycerol $n = 11$, IHx glycerol-triacetate $n = 13$; biological replicates). **e** Recognition index on the novel object recognition test after a 12-hour delay for P30 Nx and IHx mice treated with glycerol or glycerol-triacetate (Nx glycerol $n = 15$, Nx glycerol-triacetate $n = 25$, IHx glycerol $n = 16$, IHx glycerol-triacetate $n = 19$; biological replicates). **f** Violin plot showing brain weight in Nx and IHx mice of both sexes treated with glycerol or glycerol-triacetate at P30. Violin plots show the distribution, median, and upper and lower interquartile range (Nx glycerol $n = 13$, Nx glycerol-triacetate $n = 17$, IHx glycerol $n = 16$, IHx glycerol-triacetate $n = 19$; biological replicates). **g** Total lipid extracted per mg of hippocampus expressed as % from P30 Nx and IHx mice treated with glycerol or glycerol-triacetate (Nx glycerol $n = 12$, Nx glycerol-triacetate $n = 11$, IHx glycerol $n = 11$, IHx glycerol-triacetate $n = 17$; biological replicates). **h**–**l** Total fatty acids quantified by gas chromatography with tandem mass spectrometry (GC/MS) in Nx and IHx hippocampus from (**h**, **i**, **k**) male and (**h**, **j**, **l**) female P30 mice treated with glycerol or glycerol-triacetate (male: Nx glycerol $n = 6$, Nx glycerol-triacetate $n = 5$, IHx glycerol $n = 5$, IHx glycerol-triacetate $n = 7$; female: Nx glycerol $n = 6$, Nx glycerol-triacetate $n = 6$, IHx glycerol $n = 6$, IHx glycerol-triacetate $n = 10$; biological replicates). **h** Heatmap of % fatty acids from total fatty acids mean z-scores. Content of (**i**, **j**) total and (**k**, **l**) ≥20 carbon saturated and ω−9 fatty acids in males. Data points (circles/triangles) represent ug of FA/total lipid and bars represent % of total fatty acids. Black * is significantly different as ug of FA/total lipid and grey * as % of total fatty acids. For all except (**f**, **h**) data are presented as mean ± SEM. Statistical analysis for all data by 2-Way ANOVA with uncorrected Fisher's LSD post-hoc. *$p < 0.05$ (For (**a**, **b**) $p = <0.0001$, for (**d**) Nx vs IHx: glycerol $p = <0.0001$, glycerol-triacetate $p = 0.0022$; glycerol vs glycerol triacetate: IHx $p = <0.0001$, for (**e**) Nx vs IHx: glycerol $p = <0.0001$, glycerol-triacetate $p = 0.0167$; glycerol vs glycerol triacetate: IHx $p = <0.0001$, for (**f**) Nx vs IHx: glycerol $p = <0.0001$, glycerol-triacetate $p = 0.0211$, for (**g**) glycerol vs glycerol triacetate: IHx $p = 0.0087$, (**i**) Saturated/Total FA (%) $p = 0.0099$, ω−9/Total FA (%) (Nx vs IHx: glycerol $p = <0.0001$, glycerol-triacetate $p = 0.0013$; glycerol vs glycerol-triacetate: Nx $p = 0.0011$, IHx $p = <0.0001$), for (**j**) ω−9/Total FA (%) (Nx vs IHx: glycerol $p = 0.0105$; glycerol vs glycerol-triacetate: IHx $p = 0.0127$), for (**k**) ≥20 C Saturated/Total FA (%) (Nx vs IHx: glycerol $p = 0.0016$; glycerol vs glycerol-triacetate: IHx $p = 0.0002$), ≥20 C ω−9/Total Lipid (ug) (Nx vs IHx: glycerol $p = 0.0342$, glycerol-triacetate $p = 0.0415$), ≥20 C ω-9/Total FA (%) (Nx vs IHx: glycerol $p = <0.0001$, glycerol-triacetate $p = 0.0129$; glycerol vs glycerol-triacetate: Nx $p = 0.0053$, IHx $p = <0.0001$), and for (**l**) ≥20 C Saturated/Total FA (%) (Nx vs IHx: glycerol $p = 0.006$; glycerol vs glycerol-triacetate: IHx $p = 0.0019$), ≥20 C ω9/Total FA (%) (Nx vs IHx: glycerol $p = 0.0031$; glycerol vs glycerol-triacetate: IHx $p = 0.0007$). In (**h**) * represents group effect (Nx vs IHx), & treatment effect (glycerol vs glycerol triacetate), and # interaction. Glc glucose, Ac acetate, DPM disintegrating parts per million, F, fatty acids. Source data are provided as a Source Data file. Panel (**c**) was created in BioRender. Scafidi, S. (2025) https://BioRender.com/02n78cl.

differences. Specifically, females after IHx had lower levels of blood glucose and brain glucose uptake compared to Nx at P11 and subsequently normalized. Clinical data show that preterm girls (gestational age ~27.2 weeks) have higher insulin secretion compared to preterm boys with similar blood glucose levels[55]. In contrast to the adult brain, the developing brain is able to use ketones for energy and metabolism. Interestingly at P17 (6 days post-injury) we observe increased blood levels of βHB in the IHx group and comparable NEFA levels to Nx. Overall, despite reduced body weight gain, the delivery of substrates for brain de novo lipogenesis and metabolism was not compromised.

The developing brain is known to extensively utilize glucose as well as alternative substrates such as ketones and lactate for energy and metabolism[28,29]. In this study, we examined the oxidation of these alternative substrates (lactate, βHB, glutamine, and fatty acids) in the hippocampus. Here we show that only fatty acid oxidation was dramatically upregulated immediately after IHx (P11), and was sustained at P17 (6 days post-injury). This increase in fatty acid oxidation was not affected by the increased concentrations of available glucose for oxidation. The oxidation of the other alternative substrates (lactate, βHB, and glutamine) was not altered compared to Nx controls. Surprisingly, the addition of the alternative fuel acetate spared fatty acids from oxidation. For decades, it has been known that acetate is extensively metabolized by glia, specifically astrocytes[56–58]. Recent studies challenged this notion and demonstrated that neurons are also capable of utilizing acetate for energy and metabolism[58]. Therefore, acetate can serve as a potential intervention to rescue dysregulated lipid metabolism and diminish fatty acid oxidation following neonatal brain injury from intermittent hypoxemia.

Clinically and in in vivo animal models, acetate cannot be administered on its own; it has to be delivered as either sodium or potassium acetate and is usually administered intravenously[59]. The concern is that in very vulnerable EPT infants, the sodium or potassium may cause a significant metabolic and electrolyte disturbance[60,61]. Glycerol-triacetate is an alternative approach to administer acetate in vivo. It is an FDA-approved compound that provides acetate and can be administered by enteral route, is readily absorbed in the gut, and is considered generally regarded as safe (GRAS). Previous preclinical studies have shown that administration of glycerol-triacetate resulted in increased levels of acetate in blood and brain while clinical studies in infants reported no adverse events with glycerol-triacetate administration[34,62]. Here we showed that administration of glycerol-triacetate via gavage during the acute recovery (P11 to P17), led to improved performance in hippocampal-dependent behavioral test and hippocampal total lipid fatty acid profile. Specifically, the levels of endogenously synthesized ≥20 carbon-long fatty acids were recovered in IHx mice treated with glycerol-triacetate. Therefore, administration of glycerol-triacetate may rescue brain lipid metabolism during a critical period of brain development and prevent cognitive delays associated with intermittent hypoxemia in infants born EPT.

Methods

Animals

Animal experiments were approved by the Institutional Animal Care and Use Committee (IACUC) at Johns Hopkins School of Medicine in accordance with the guidelines and regulations of the NIH *Guide for the Care and Use of Laboratory Animals* (protocol #MO23K317). C57BL/6 wild-type mice (*Mus musculus*) were purchased from the Jackson Laboratory (Jackson ID #000664); *Cpt2*$^{lox/lox}$ conditional mice from Dr. Michael J. Wolfgang[63] (C57BL/6 genetic background) were bred to *Nestin*- or *Gfap*-Cre transgenic mice (Jackson ID #003771; B6.Cg-Tg(Nes-cre)1Kln/J and #024098; B6.Cg-Tg(Gfap-cre)77.6Mvs/2 J) to generate pan-brain (*Cpt2*$^{B-/-}$) or astrocyte-specific (*Cpt2*$^{G-/-}$) knockout mice. Mice were bred in-house and the colonies maintained in the animal facility of Johns Hopkins University School of Medicine in ventilated racks with a 12-hour light/dark cycle in a temperature (20-25 °C) and humidity (30–70%) controlled room, and had *ad libitum* access to water and standard chow (5v75 - PicoLab Verified 75 IF, Lab Diet).

Intermittent hypoxia

Postnatal day (P)1 pups were randomized to undergo intermittent hypoxia (IHx) or serve as normoxia (Nx) controls, removed from the dam, and placed in sealed containers (Coy Laboratories) at ambient temperature. IHx pups were exposed to 16 cycles of brief 3 min episodes of hypoxia (8% O_2) followed by 5 min of re-oxygenation to 21% FiO_2. Nx pups were exposed to 16 cycles of regular air. The pups were

returned to their dam for 2 h, and the 16 cycles of Nx or IHx were repeated. These 32 cycles in total were repeated daily for 11 days until P11. Pups from different litters and from both sexes were used for each experiment and were assessed at P11, P17, P22, and P30 unless otherwise stated. Data from males and females was reported as combined, male only, and female only. The hippocampus was selected a priori for microdissection and analysis due to its role in learning and memory, and its susceptibility to developmental disruption in children EPT. Blood glucose and lactate levels were determined using blood glucose and lactate meters (Nova Abbott). Blood was collected in 5% 0.5 M EDTA, and plasma β-hydroxybutyrate (StanBio; 2440) and non-esterified fatty acids (NEFA) (Wako; 999-35691, 999-34791, 999-34891, 999-35191, 276-76491) were measured as per manufacturer's instructions.

Glycerol-triacetate treatment

Normoxia and IHx-injured mice were randomized at P11 to receive vehicle (glycerol, Millipore Sigma; G5516) or glycerol-triacetate (Triacetin, Millipore Sigma; 1030001000). Glycerol or glycerol-triacetate was administered by oral gavage (5 mg/g body weight) daily from P11 to P17.

Human samples

Human hippocampus was obtained from the National Institutes of Health (NIH) NeuroBioBank at University of Maryland, Baltimore, MD, United States (ID #3243). Donors consisted of ~1.6 months-old (average) infants born at term (38–40 weeks; $n = 4$) and infants born extremely premature (≤ 28 weeks; $n = 3$) with a corrected average age of ~1-month. Both sexes, male and female, were included in this study. None of the donors had a history of hypoxia ischemia, severe infection, or known genetic diseases. Frozen tissues were stored at −80 °C.

Gene expression

Total RNA from microdissected hippocampal tissue ($n = 8$/sex/age/group) was extracted using TRIzol (Life Technologies; 15596018), and further purified using the RNeasy Plus Mini Kit (Qiagen; 74134). RNA was quantified by NanoDrop One spectrophotometer (Thermo Fisher Scientific) and converted to cDNA with the High Capacity cDNA Reverse Transcriptase kit (Applied Biosystems; 4368814). Real-Time PCR was performed using 10 ng of cDNA, SsoAdvanced Universal SYBR Green Supermix (Bio-Rad; 1725271), and primers for the target genes (Supplementary Table 18), and analyzed using the CFX Opus 96 machine (Bio-Rad). Data was normalized to the average Ct values of the housekeeping genes (18S, Ppia, Ywaz, and Osbp) and expressed as arbitrary units of $2^{-\Delta Ct}$.

To determine the mitochondrial DNA (mtDNA) content relative to nuclear DNA, genomic DNA was isolated from microdissected hippocampus using a QiAmp DNA Mini kit (Qiagen, #51304). EvaGreen-based digital PCR was performed by the Johns Hopkins University School of Medicine Genetic Resources Core Facility (RRID:SCR_018669) using samples as a template and primers to amplify the mitochondrial target genes, cytochrome c oxidase I (*Co1*) and NADH dehydrogenase 1 (*Nd1*), and the nuclear target gene *H19* (Supplementary Table 18). Biological replicates were tested in duplicate using an 8500 partition nanoplate (Qiagen #250021) in a QIAcuity 8; Firmware version 3.1 instrument (Qiagen) according to the manufacturer's recommendations for EvaGreen. Each assay was run independently. Samples were run at 10 ng/ul concentration for the *H19* gene and at a 1:100 dilution for the mitochondrial genes. 5 ul of the sample at the appropriate concentration was added to 7.2 ul of master mix. 12.2 ul of master mix was loaded into the nanoplate, and the instrument delivered 2.6 ul of the total to be partitioned across each well. Results were analyzed with the QIAcuity Digital Suite v3.1.0.0 software (Qiagen). Concentrations were adjusted for all dilution levels within the software and are reported as copies/ul in the original 10 ng/ul sample tube.

Proteomics

16-plex-TMTpro experiment was performed by the Johns Hopkins Mass Spectrometry and Proteomics Facility. Hippocampal protein was extracted from frozen microdissected hippocampal tissue (total $n = 16$; $n = 4$/sex/group; biological replicates) using RIPA lysis buffer system with protease inhibitors (Santa Cruz; sc-24948). The Pierce™ BCA Protein Assay Kit (Thermo Fisher Scientific; 23227) was used to determine protein concentration according to the manufacturer's protocol. *Proteolytic Digestion:* Protein samples (50ug each) were diluted to 20 ul with 50 mM triethylammonium bicarbonate (TEAB), reduced with 5 ul 50 mM Dithiothreitol in 100 mM TEAB at 60 °C for 45 min followed by alkylating with 100 mM Chloroacetamide in 100 mM TEAB in the dark for 15 min at room temperature. A single pot, solid phase sample preparation protocol (SP3)[64] using a mixture of Sera-Mag SpeedBeads (GE Healthcare; 45152105050250 and 65152105050250) was used to remove detergents and other non-protein contaminants. The proteins bound to beads were resuspended in 100ul of 100 mM TEAB and digested with 3.4 ug of Trypsin/LysC (Pierce) overnight at 37 °C. The digested peptides were separated from the magnetic beads using a magnetic tube holder and placed into a new 0.5 ml Eppendorf centrifuge tube. *Isobaric Mass Tag Labeling:* Peptides in each of the 16 digested samples were labeled with a unique TMTpro 16-plex reagent (Thermo Fisher; LOT #WH324722) according to the manufacturer's instructions. All 16 TMT labeled peptide samples were combined and dried by vacuum centrifugation. *Peptide fractionation:* The combined TMT-labeled peptides (800ug) were aliquoted, and one aliquot of 300 ug was dried prior to off-line fractionation. Peptides were re-constituted in 2 ml 10 mM TEAB buffer and loaded on a XBridge C18 Guard Column (5 μm, 2.1 × 10 mm, Waters) at 250 μL/min for 8 min prior to fractionation on a XBridge C18 Column (5 μm, 2.1 × 100 mm column (Waters) using a 0 to 90% acetonitrile in 10 mM TEAB gradient over 85 min at 250 μL/min on an Agilent 1200 series capillary HPLC with a micro-fraction collector. Eighty-four 250ul fractions were collected and concatenated into 24 fractions according to Wang et al. 2011 and dried[65]. *Mass Spectrometry analysis:* Peptides in each of the 24 fractions were analyzed on a nano-LC-Orbitrap-Fusion Lumos-IC in FTFT mode (Thermo Fisher Scientific) interfaced with an EasyLC1100 series by reversed-phase chromatography using a 2%–90% acetonitrile in 0.1% formic acid gradient over 90 min at 300 nl/min on a 75 μm × 150 mm ReproSIL-Pur-120-C18-AQ column 3 μm, 120 Å (Dr. Maisch). Survey scans of precursor ions were acquired from 375 to 1500 *m/z* at 120,000 resolution at 200 *m/z* with automatic gain control (AGC) at 4e5 and a 50 ms maximum injection time. Precursor ions were individually isolated in a 3 second cycle time within 0.7 *m/z* by data dependent monitoring and 15 s dynamic exclusion, and fragmented using an HCD activation collision energy 36. Fragmentation spectra (MS/MS) were acquired using a 1.25e5 AGC and 86 ms maximum injection time (IT) at 50,000 resolution. *Data analysis:* Fragmentation spectra were processed by Proteome Discoverer v2.4 (PD2.4, ThermoFisher Scientific) and searched with Mascot v.2.8.0 (Matrix Science, London, UK) against RefSeq2021_204 mouse database. Search criteria included trypsin enzyme, one missed cleavage, 3 ppm precursor mass tolerance, 0.01 Da fragment mass tolerance, with TMTpro on N-terminus and carbamidomethylation on C as fixed and TMTpro on K, oxidation on M, deamidation on N or Q as variable modifications. Peptide identifications from the Mascot searches were processed within PD2.4 using Percolator at a 5% False Discovery Rate confidence threshold, based on an auto-concatenated decoy database search. Peptide spectral matches (PSMs) were filtered for Isolation Interference <30%. Relative protein abundances of identified proteins were determined in PD2.4 from the normalized median ratio of TMT reporter ions, having signal to noise ratios >1.5, from all PSMs from the same protein. *P*-values of mean protein ratios for the biological replicates were calculated using the ANOVA method. Technical variation in ratios from our mass spectrometry analysis is less than 10%[66]. *Pathway*

enrichment analysis: Pathway analysis of differentially expressed proteins (p-value < 0.05) was performed using g:Profiler (https://biit.cs.ut.ee/gprofiler/gost). g:SCS was selected as statistical threshold and p-value < 0.05 as the significance threshold. Significant pathways from Reactome were selected and the pathways belonging to the first or second hierarchical levels were plotted[67]. The proteomics data generated in this study have been deposited to the ProteomeXchange Consortium via the PRIDE[68] partner repository with the dataset identifier PXD070491.

Behavior

Novel object recognition (NOR) test and Y-Maze spontaneous alteration test. *Novel object recognition test:* The test was used to assess hippocampal-dependent recognition memory and performed as previously described in ref. 69. In brief, the open field and objects used were always cleaned with 30% ethanol (vol/vol) between each mouse to minimize olfactory cues. Prior to the testing day, P30 mice were habituated to an opaque rectangular box (27 × 27 × 20 cm) for 5 min. In the familiarization phase, mice were placed inside the box and allowed to explore two identical objects, placed equidistant from each other, for a total of 30 s or after 5 min had passed. The test was repeated 12 h later but one object was replaced with a novel object. Mice were placed inside the box and allowed to explore the objects. The experiment stopped when the mouse explored the objects for a total of 30 s. The time it took to reach the criterion of 30 s and the total time spent exploring each individual object were recorded and analyzed with the ANY-maze video tracking system (v6.3, Stoelting Co., IL). The recognition index was calculated by dividing the amount of time spent on the novel object by the total exploration time (Time in novel / 30 sec). *Y-Maze spontaneous alternation test:* The test was used to assess spatial working memory as previously described in refs. 69,70. In brief, P30 mice were placed in the center of a Y-shaped maze and allowed to freely explore the three arms (labeled as A, B, and C) for 8 minutes. The activity and arm choice were recorded with a video camera. The Y-maze was cleaned with 30% ethanol (v/v) between mice. The spontaneous alternation percentage was calculated by dividing the number of alternations (three unique arm entries) by the total number of possible triads minus one (Total alternations/[total entries − 2]) × 100. All behavioral tests were performed by the investigator blinded to groups and treatments.

Mito Fuel Flex test

The Mito Fuel Flex test (Agilent) was performed using a Seahorse XFe96 analyzer (Agilent) to measure the dependency of brain cells to oxidize glucose, glutamine, and fatty acids to maintain basal respiration. Single-cell suspensions from microdissected hippocampus were prepared using accutase. The Agilent Seahorse Technical Manual was followed to determine the rate of oxidation of each fuel by measuring the oxygen consumption rate (OCR) in the presence or absence of inhibitors for each of the specific fuel pathways. UK5099 was used as an inhibitor of glucose oxidation, etomoxir as an inhibitor of fatty acid oxidation, and BPTES as an inhibitor of glutamine oxidation. All assays were performed and analyzed in real-time by the manufacturer's software (Wave 2.6.3). The number of cells plated was analyzed with Biotek Cytation 1 (Agilent), and OCR was normalized to protein concentration in each well. The protein concentration was exported directly to the Agilent Seahorse, and raw data was normalized to account for differences in protein concentration within each well.

Lipidomics

Frozen mouse microdissected hippocampal tissue or human hippocampal tissue (Mouse tissue -total $n = 48$; $n = 6$/age/group, biological replicates; human tissue – total $n = 7$, term/control $n = 4$, preterm $n = 3$; biological replicates) were homogenized with PBS buffer at a concentration 100 mg/ml. The total lipid extracts of the brain tissue were prepared using a revised MTBE lipid extraction method[71]. Briefly, 10 ul of brain homogenate, 400 ul of ice-cold methanol, and 10ul of internal standard (EquiSPLASH, Avanti Polar Lipids, Alabaster, AL) were combined, vortex mixed for 30 s, and then incubated at 4 °C for 10 min with 650 rpm shaking. Next, 500 ul of ice-cold MTBE was added, vortex mixed for 30 s and incubated at 4 °C for 1 h with 650 rpm shaking. After incubat ion, 500 ul of ice-cold H_2O was added, vortex mixed for 30 s and incubated at 4 °C for 15 min with 650 rpm shaking. The mixture was then centrifuged at 8000 g for 8 min at 4 °C, and the top organic layer was collected and stored on ice. An additional 200 ul of MTBE was added to the aqueous phase, vortex mixed for 30 s, incubated at 4 °C for 15 min, and centrifuged at 8000 g for 8 min at 4 °C. The organic layer was collected and combined with the previous extract. The collected organic layer was dried under N_2 gas and re-suspended in 200 ul of $CHCl_3$/MeOH (1:1, v/v) containing 200 uM of butylated hydroxytoluene (BHT) and stored at −20 °C until analysis. Samples were further diluted with IPA/ACN/H2O (2:1:1 v/v) prior to analysis. The total protein content was measured with a Pierce™ BCA Protein Assay Kit (Thermo Fisher Scientific, Rockford, USA) according to the manufacturer's protocol, and used for the data normalization.

The liquid chromatography, tandem mass spectrometry (LC-MS/MS) analysis was conducted on an Ultimate 3000 Ultra High-Performance Liquid Chromatograph (UHPLC) coupled to a Thermo TSQ Altis Tandem Quadrupole Mass Spectrometer (Thermo Scientific, San Jose, CA). Chromatographic separation was achieved with an ACQUITY Amide BEH column (1.7 µm, 2.1 × 100 mm) maintained at 45 °C (Waters, Milford, MO). Mobile phase compositions for solvents A and B consisted of ACN/H2O (95:5, v/v) and (50:50, v/v) respectively, with 10 mM ammonium acetate. The gradient profile had a flow rate of 0.6 ml min^{-1} and ramped from 0.1 to 20% B in 2 min, from 20 to 80% B in 3 min, dropped from 80 to 0.1% B in 0.1 min, and held 0.1% B for 2.9 min. Total chromatographic run time was 8.0 min. The injection volume was 2 ul. All analytes were detected using negative or positive ionization mode and selection reaction monitoring (SRM) library were adopted from Medina et al.[72]. The SRM is a targeted method that uses predetermined chromatographic retention times and precursor-to-product ion transitions to detect and identify each lipid, and has been implemented in our previously published studies[73–75]. Data were acquired using spiked-in internal standards (Avanti Polar Lipids EquiSPLASH, #330731) which provided one deuterium stable-labeled lipid per lipid class. The lipid standards allowed for compensation during lipid extraction and ionization efficiency. Collision energies and RF lens voltage were optimized for each reference standard. Data acquisition was performed using Xcalibur software v4.2 (Thermo Scientific, San Jose, CA) and processed using TraceFinder 5.1 (Thermo Scientific, San Jose, CA). Peak area was determined using ICIS peak peaking algorithm and 7-point smoothing. All peak area integration was manually verified. The peaks areas were then normalized to sum composition, mean-centered, and log-transformed using MetaboAnalyst 6.0 (https://www.metaboanalyst.ca/)[76]. The data as presented represent abundances rather than concentrations, enabling visualizing of hundreds of detected lipids with multivariate and univariate statistical analyses. Additional data analysis was done using MetaboAnalyst 6.0 and Prism 10 (GraphPad, La Jolla, CA). The lipidomics data generated in this study have been deposited in the Mendeley Data Repository under the https://doi.org/10.17632/nzwvkr7vgj.1[77].

Total Lipid Fatty Acid Analyses

Chemicals, reagents, and materials used for the lipid extractions and fatty acid analyses were of the highest quality available. MilliQ water, filtered deionized water is available in the laboratory. Methanol, optima grade was obtained from Thermo Fisher Scientific (Fair Lawn,

NJ). Chloroform, HPLC grade was from Burdick & Jackson (Muskegan, MI), Stable-isotope-labeled internal standards (deuterated); were purchased from Cambridge Isotope Laboratories, Andover MA (internal standards C27:0 and C19:0; deuterium fatty acids, C8:0, 10:0, 12:0, 14:0, 15:0, 16, 18:0, 20:0, 22:0) or CDN Isotopes, Quebec, CAN (deuterium fatty acids C24:0, 26:0, pristanic and phytanic). Natural fatty acid standards were purchased from Nu Chek Prep (Elysian, MN) and were checked for purity by capillary gas chromatography by analysis on two capillary columns, a non-polar, DB1, and a polar, SP2560, capillary columns (50 m × 0.25 mm × 0.2 μm) purchased from Supelco, Sigma-Aldrich, Inc, St. Louis, MO.

Frozen microdissected hippocampal tissues (total $n = 142$; P11: male Nx $n = 4$, IHx $n = 5$, female Nx $n = 6$, IHx $n = 5$; P17: male Nx $n = 5$, IHx $n = 6$, female Nx $n = 6$, IHx $n = 7$; P22: male Nx $n = 6$, IHx $n = 5$, female $n = 6$/group; P30: $n = 6$/sex/group; P30 glycerol/glycerol-triacetate experiment - male: Nx glycerol $n = 6$, Nx glycerol-triacetate $n = 5$, IHx glycerol $n = 5$, IHx glycerol-triacetate $n = 7$; female: Nx glycerol $n = 6$, Nx glycerol-triacetate $n = 6$, IHx glycerol $n = 6$, IHx glycerol-triacetate $n = 10$; biological replicates) were weighed (0.1 to 0.2 g) and extracted with chloroform: methanol 2:1, v/v according to Folch et al.[78]. Total lipids were dried under N_2 and weighed. The lipids were solubilized in 1 ml chloroform: methanol 2:1, and approximately 1 mg lipid from each sample was transferred to a 13 x 100 mm screw capped test tube for analysis of total lipid fatty acids, including saturated, monounsaturated, and polyunsaturated of chain length C10 to C30. Fatty acids were hydrolyzed from triglycerides and phospholipids in a two-step process of acidification with 90:10 v:v acetonitrile:6 N HCl and neutralization with 90:10 v:v methanol:10 N NaOH, with incubations at 104 °C for 45 min, then reacidified in 6 N HCl. Total fatty acids were extracted in hexane then derivatized with triethylamine and pentafluorobenzyl bromide (in acetonitrile) at room temperature 15 min[79,80]. The resulting pentaflourobenzyl bromide esters were separated and quantified by capillary gas chromatography electron capture negative ion mass spectrometry (GCMS) by the method of Lagerstedt et al.[81] except that a 50 m × 0.25 mm × 0.2 μm SP2560 column was used for analysis. All fatty acids were analyzed on an Agilent 7890 A GC coupled to a 5975 C mass selective detector (MSD), with helium as the carrier gas and ammonia as the reagent gas. After a 1 μl 1:35 split injection, the oven temperature was ramped more slowly at lower temperatures in two steps, resulting in a total run time of 55 min. The initial oven temperature of 60 °C was held for 2 min, then increased at 10 °C/min to 180 °C, followed by a slower ramp at 2.5 °C/min to 250 °C, and then held for 14 min. The MSD transfer line was initially maintained at 240 °C for 33 minutes, then increased at 2.5 °C/min to a final temperature of 250 °C and held for an additional 32 min. Data were acquired in select ion monitoring (SIM) mode, with dwell times ranging from 50 ms to 100 ms per ion species. Each analyte was matched to one of 13 stable-isotope labeled internal standards with the closest chain length and retention time. The fatty acids were quantitated using the Agilent MSD Chem Station software G1701EA version E.02.02.1431. The fatty acid retention time and peak integration were checked and each fatty acid was measured using a standard curve that was assayed with each set of analyses. For quality control, a reagent blank, a normal, and an abnormal plasma control samples were assayed with each set of analyses. Results were transferred into Excel for the final calculations as fatty acid ug/mg lipid weight.

Acylcarnitines

Acylcarnitines levels in the blood (total $n = 62$; male: P11, P17, and P22 $n = 4$/group; P30 Nx $n = 4$, IHx, $n = 5$; female: P11 Nx $n = 4$, IHx $n = 3$; P17 $n = 4$/group; P22 Nx $n = 4$, IHx, $n = 3$; P30 Nx $n = 3$, IHx $n = 4$; biological replicates) were quantified from dried blood spots (DBS) following a previously described method with modifications[3,4]. In brief, punched 1/8″ DBS samples were transferred into tubes containing 100 ul of methanol and internal standards for acylcarnitines (NSK B; Cambridge Isotopes). Samples were incubated at 4 °C for 20 min and then dried under nitrogen. The dried samples were resuspended in 60 μl 3 N HCl in *n*-butanol and incubated at 65 °C for 15 min. Afterward, samples were dried under nitrogen and the residue containing butylated acylcarnitines was reconstituted in 100ul of mobile phase acetonitrile/water/formic acid (H2O:CH3CN:HCOOH; 80:19.9:0.1 v/v%). Samples were vortexed, transferred to a centrifuge filter, and spun. The filtrates were then transferred to injection vials.

Acylcarnitines from frozen hippocampus (total $n = 63$; male: P11, P17, and P22 $n = 4$/group; P30 Nx $n = 4$, IHx, $n = 5$; female: P11 Nx $n = 5$, IHx $n = 3$; P17 $n = 4$/group; P22 Nx $n = 4$, IHx, $n = 3$; P30 Nx $n = 3$, IHx $n = 4$; biological replicates) were extracted by homogenizing the tissue in a solution of methanol containing the acylcarnitine standards. Samples were sonicated at room temperature for 10 min and then centrifuged at 16,200 × g for 4 min at 4 °C. After centrifugation, the liquid phase was transferred to a glass tube, evaporated under nitrogen, and processed as described above. Analysis of acylcarnitines was performed using an API 4500 mass spectrometer (AB SCIEX, Foster City, CA) operated in the positive-ion mode employing precursor ion scan for *m/z* 85, a characteristic product ion of butyl ester of acylcarnitine species. Data was processed using the ChemoView 2.0.2 (AB SCIEX) application. Blood samples are reported as nmol/ml and tissue samples as pmol/mg.

MALDI-MSI

MALDI MSI experiments were performed by the Johns Hopkins Applied Imaging Mass Spectrometry (AIMS) Core. All solvents and MALDI matrices were purchased from Sigma Aldrich (St. Louis, MO) and were used without further purification. All solvents were of HPLC grade or higher. *Sample preparation:* Brain samples from Nx and IHx P17 male mice were collected immediately after sacrifice and frozen using liquid nitrogen vapors (total $n = 8$; $n = 4$/group). Samples were stored at −80 °C before cryosectioning. 10 μm thick sagittal brain sections were collected using a Leica CM1860 UV Cryostat (Leica Biosystems, Wetzlar, Germany) and depth was verified by comparing tissue morphology to Allen Brain Atlas images at the target depth. Sections were thaw-mounted onto indium-tin oxide (ITO) coated glass microscope slides (Delta Technologys, Loveland, CO) and stored at −80 °C prior to matrix application. *Matrix application:* Slides were warmed to room temperature in a vacuum desiccator, then sprayed with 5 mg/mL α-cyano-4-hydroxycinnamic acid (CHCA) in 70% acetonitrile with 0.1% trifluoroacetic acid using an HTX M3+ pneumatic matrix sprayer (HTX Technologies, Chapel Hill, NC). Matrix was sprayed at 100 μL / min for 8 passes using a 60 °C nozzle temperature, 10 psi nitrogen pressure, 1350 mm/min nozzle velocity, 3 mm track spacing, and 10 second drying time. *MALDI-MSI data acquisition*: Immediately after matrix deposition, slides were imaged using a Bruker timsTOF FleX MALDI-2 mass spectrometer (Bruker Daltonics, Billerica, MA) equipped with a SmartBeam 3D 10 kHz Nd:YAG laser at 355 nm with beam scan enabled and a 46 um scan range. Height adjustment and laser focus tuning were performed prior to mass calibration. Mass calibration was performed using electrospray ionization (ESI) of Agilent ESI-L Tune Mix, resulting in a mass error <1 PPM. Instrument parameters were optimized to maximize intensity, as described in Supplementary Table 19. Data were acquired for *m/z* 100–950 in positive ion mode using a 50 μm raster width with 1 burst of 225 laser shots per pixel. On-tissue MS/MS analysis was conducted by switching the instrument to MS/MS mode and collecting 5 summed bursts of 250 shots from the hippocampus of Nx and IHx samples for the parent and fragment spectra of each species of interest (Supplementary Figs. 10,11). Parent ions were searched against the Lipid Maps database[82–84]. *MALDI MSI data analysis:* MALDI MSI data were imported into SCiLS Lab (version 2023b, Bruker Daltonics, Bremen, Germany). Data were normalized using total ion current (TIC) and analyzed using SCiLs lab's feature finding and hypothesis testing workflows.

In-vivo metabolite uptake

Glucose uptake into the brain was measured using [1,2-^{3}H]-2-Deoxy-D-glucose (2-DG) (Moravek Biochemicals; MT911), an unmetabolizable analog of glucose that enters cells but becomes trapped after phosphorylation. Mice were injected intraperitoneal (i.p.) with 0.2uCi/g of 2-DG diluted in sterile saline. Brains were harvested 45 minutes after injection. Tissue from microdissected hippocampus was extracted using ice-cold 7% perchloric acid and centrifuged at 14,000 g for 15 min at 4 °C. The supernatant was transferred to a vial containing scintillation fluid (National Diagnostics; LS-270) and radioactivity was measured in a LS 6500 Multi-purpose Scintillation Counter (Beckman Counter, Inc. USA). Disintegrations per minute (DPM) counts were normalized to wet tissue weight.

Fatty acid uptake into the hippocampus was measured using [1-^{14}C]-2-Bromopalmitate (2-BP, Moravek Biochemicals; MC451). Mice were injected intraperitoneal (i.p.) with 0.2uCi/g of 2-BP complexed to bovine serum albumin and diluted in sterile saline. Microdissected hippocampus were harvested 45 minutes after injection. Total lipids were extracted using the Folch method and transferred to vials containing scintillation liquid to measure radioactivity in a LS 6500 Multi-purpose Scintillation Counter (Beckman Counter, Inc. USA)[78]. DPM counts for ^{14}C were normalized to wet tissue weight.

Ex-vivo oxidation studies

Oxidation assays were measured in stoppered tubes containing a center well with Whatman filter paper as previously described in refs. 3,4,85. In brief, the hippocampal region was microdissected and placed into tubes with labeling media containing either [1-^{14}C]-oleic acid (Moravek Biochemicals; MC406), [U-^{14}C]-D-glucose (Moravek Biochemicals; MC144W), [U-^{14}C]-glutamine (Moravek Biochemicals; MC1124), [U-^{14}C]-L-lactic acid (PerkinElmer; NEC599050UC), [3-^{14}C]-D−3-Hydroxybutyric acid, (American Radiolabeled Chemicals, Inc; ARC#4122), or [1,2-^{14}C]-acetic acid (PerkinElmer; NEC553050UC) and incubated in a 37 °C water bath with gentle shaking for 3 h. Labeling media was composed of 20% neurobasal medium (Gibco; 21103-049), 80% DMEM (Gibco; A14430), 0.5 mM L-carnitine (Sigma; C0283), 0.2% bovine serum albumin (BSA; Sigma; A9647), and 25 µM glutamine (Gibco; 25030). 100 µM Etoximir (Sigma; E1905) was added to the media of the treated samples at the beginning of the assay as control for the [1-^{14}C]-oleic acid oxidation assay. $^{14}CO_2$ from complete substrate oxidation was trapped by the addition of 200 µl of 1 M perchloric acid in the medium and 150 µl of 1 M NaOH to the center well containing the filter paper and incubating the samples at 55 °C for 1 hour. The filter paper was transferred to a vial containing scintillation fluid and the radioactivity was counted 24 h later. 1 ml of acidified media was collected to measure acid-soluble metabolites, products from incomplete [1-^{14}C]-oleic acid oxidation. 60 µl of BSA and 100 ul of 1 M perchloric acid were added to the media and incubated overnight at 4 °C. The next day, samples were centrifuged at 1467 × g for 30 min, the supernatant was transferred to vials containing scintillation fluid, and radioactivity was measured in a LS 6500 Multi-purpose Scintillation Counter (Beckman Counter, Inc. USA). DPM counts for $^{14}CO_2$ and ^{14}C-ASM were normalized to specific activity and wet tissue weight.

Lipid synthesis

Acetate incorporation into total lipid fraction was performed using [^{3}H]-Acetate[85,86]. The microdissected hippocampal region was incubated at 37 °C for 3 h with 1uCi [^{3}H]-Acetate (Moravek Biochemicals; MT634) in the same media composition used for the oxidation assays. Total lipids were extracted using the Folch method and transferred to vials containing scintillation fluid to measure radioactivity in a LS 6500 Multi-purpose Scintillation Counter (Beckman Counter, Inc. USA)[78]. DPM counts for ^{3}H were normalized to wet tissue weight.

Data and statistical analysis

Data are shown as the mean ± SEM for each group unless otherwise stated. Data were analyzed using Prism 10 software (GraphPad, La Jolla, CA). Additional data analysis was performed using MetaboAnalyst 6.0[76]. The statistical significance was determined using the 2-tailed Mann–Whitney test or unpaired Student's t-test at instances where the total sample size was ≤7, 2-tailed paired t-test, and 2-way ANOVA with uncorrected Fisher's LSD post-hoc. Statistical significance was set at $p < 0.05$. Correlation analysis was performed using simple linear regression.

Artwork

Experimental design figures and biochemical pathways figures were created with BioRender.com full license plan.

Reporting summary

Further information on research design is available in the Nature Portfolio Reporting Summary linked to this article.

Data availability

The proteomics data generated in this study have been deposited to the ProteomeXchange Consortium via the PRIDE[68] partner repository with the dataset identifier PXD070491. The lipidomics data generated in this study have been deposited in the Mendeley Data Repository under the DOI: 10.17632/nzwvkr7vgj.1[77]. All other data generated in this study are provided in the Supplementary Information and the Source Data file. Source data are provided with this paper.

References

1. Aeberhard, E., Grippo, J. & Menkes, J. H. Fatty Acid Synthesis in the Developing Brain. *Pediatr. Res* **3**, 590–596 (1969).
2. Volpe, J. J., Lyles, T. O., Roncari, D. A. & Vagelos, P. R. Fatty acid synthetase of developing brain and liver. Content, synthesis, and degradation during development. *J. Biol. Chem.* **248**, 2502–2513 (1973).
3. White, C. J. et al. Determining the Bioenergetic Capacity for Fatty Acid Oxidation in the Mammalian Nervous System. *Mol. Cell. Biol.* **40**, e00037-20 (2020).
4. Jernberg, J. N., Bowman, C. E., Wolfgang, M. J. & Scafidi, S. Developmental regulation and localization of carnitine palmitoyltransferases (CPT s) in rat brain. *J. Neurochem.***142**, 407–419 (2017).
5. Jarjour, I. T. Neurodevelopmental Outcome After Extreme Prematurity: A Review of the Literature. *Pediatr. Neurol.* **52**, 143–152 (2015).
6. Martin, R. J., Wang, K., Köroğlu, Ö, Di Fiore, J. & Kc, P. Intermittent Hypoxic Episodes in Preterm Infants: Do They Matter? *Neonatology* **100**, 303–310 (2011).
7. Di Fiore, J. M. et al. Prematurity and postnatal alterations in intermittent hypoxaemia. *Arch. Dis. Child Fetal Neonatal Ed.* **106**, 557–559 (2021).
8. Janvier, A. et al. Apnea Is Associated with Neurodevelopmental Impairment in Very Low Birth Weight Infants. *J. Perinatol.* **24**, 763–768 (2004).
9. Poets, C. F. et al. Association Between Intermittent Hypoxemia or Bradycardia and Late Death or Disability in Extremely Preterm Infants. *JAMA* **314**, 595 (2015).
10. Williamson, M., Poorun, R. & Hartley, C. Apnoea of Prematurity and Neurodevelopmental Outcomes: Current Understanding and Future Prospects for Research. *Front. Pediatr.* **9**, 755677 (2021).
11. White, T. A., Miller, S. L., Sutherland, A. E., Allison, B. J. & Camm, E. J. Perinatal compromise affects development, form, and function of the hippocampus part one; clinical studies. *Pediatr. Res* **95**, 1698–1708 (2024).
12. Isaacs, E. B. et al. Hippocampal Volume and Everyday Memory in Children of Very Low Birth Weight. *Pediatr. Res* **47**, 713–720 (2000).

13. Cooper, J. M. et al. Neonatal Hypoxia, Hippocampal Atrophy, and Memory Impairment: Evidence of a Causal Sequence. *Cereb. Cortex* **25**, 1469–1476 (2015).
14. Salmaso, N., Jablonska, B., Scafidi, J., Vaccarino, F. M. & Gallo, V. Neurobiology of premature brain injury. *Nat. Neurosci.* **17**, 341–346 (2014).
15. Juliano, C. et al. Mild intermittent hypoxemia in neonatal mice causes permanent neurofunctional deficit and white matter hypomyelination. *Exp. Neurol.* **264**, 33–42 (2015).
16. Semple, B. D., Blomgren, K., Gimlin, K., Ferriero, D. M. & Noble-Haeusslein, L. J. Brain development in rodents and humans: Identifying benchmarks of maturation and vulnerability to injury across species. *Prog. Neurobiol.* **106–107**, 1–16 (2013).
17. Cottam, N. C. et al. From Circuits to Lifespan: Translating Mouse and Human Timelines with Neuroimaging-Based Tractography. *J. Neurosci.* **45**, e1429242025 (2025).
18. Cha, J. H. et al. Growth Trajectories of Children Born Preterm and Full-Term With Low Birth Weight to Preschool Ages: A Nationwide Study. *J. Clin. Endocrinol. Metab.* **110**, e283–e293 (2025).
19. Greenbury, S. F. et al. Birthweight and patterns of postnatal weight gain in very and extremely preterm babies in England and Wales, 2008–19: a cohort study. *Lancet Child Adolesc. Health* **5**, 719–728 (2021).
20. Vinther, J. L. et al. Gestational age and trajectories of body mass index and height from birth through adolescence in the Danish National Birth Cohort. *Sci. Rep.* **13**, 3298 (2023).
21. Yoshida-Montezuma, Y. et al. Late preterm birth and growth trajectories during childhood: a linked retrospective cohort study. *BMC Pediatr.* **23**, 450 (2023).
22. Patel, M. S. & Tonkonow, B. L. Development of lipogenesis in rat brain cortex: the differential incorporation of glucose and acetate into brain lipids in vitro. *J. Neurochem.* **23**, 309–313 (1974).
23. Saito, M., Chakraborty, G., Mao, R.-F., Vadasz, C. & Saito, M. Developmental Profiles of Lipogenic Enzymes and Their Regulators in the Neonatal Mouse Brain. *Neurochem Res* **34**, 1945–1954 (2009).
24. Smith, M. E. et al. Upregulated hepatic lipogenesis from dietary sugars in response to low palmitate feeding supplies brain palmitate. *Nat. Commun.* **15**, 490 (2024).
25. Rapoport, S. I. In Vivo Fatty Acid Incorporation into Brain Phospholipids in Relation to Signal Transduction and Membrane Remodeling. *Neurochem Res* **24**, 1403–1415 (1999).
26. Clandinin, M. T., Chappell, J. E., Heim, T., Swyer, P. R. & Chance, G. W. Fatty acid utilization in perinatal de novo synthesis of tissues. *Early Hum. Dev.* **5**, 355–366 (1981).
27. Kim, H.-Y., Huang, B. X. & Spector, A. A. Phosphatidylserine in the brain: Metabolism and function. *Prog. Lipid Res.* **56**, 1–18 (2014).
28. Bowman, C. E., Scafidi, J. & Scafidi, S. Metabolic perturbations after pediatric TBI: It's not just about glucose. *Exp. Neurol.* **316**, 74–84 (2019).
29. McKenna, M. C., Scafidi, S. & Robertson, C. L. Metabolic Alterations in Developing Brain After Injury: Knowns and Unknowns. *Neurochem Res* **40**, 2527–2543 (2015).
30. Bowman, C. E. & Wolfgang, M. J. Role of the malonyl-CoA synthetase ACSF3 in mitochondrial metabolism. *Adv. Biol. Regul.* **71**, 34–40 (2019).
31. Morant-Ferrando, B. et al. Fatty acid oxidation organizes mitochondrial supercomplexes to sustain astrocytic ROS and cognition. *Nat. Metab.* **5**, 1290–1302 (2023).
32. Honda, A. et al. Very-long-chain fatty acids are crucial to neuronal polarity by providing sphingolipids to lipid rafts. *Cell Rep.* **42**, 113195 (2023).
33. Wang, Y. et al. The multiple facets of acetyl-CoA metabolism: Energetics, biosynthesis, regulation, acylation and inborn errors. *Mol. Genet. Metab.* **138**, 106966 (2023).
34. Segel, R. et al. A safety trial of high dose glyceryl triacetate for Canavan disease. *Mol. Genet. Metab.* **103**, 203–206 (2011).
35. Allen, M. C., Cristofalo, E. A. & Kim, C. Outcomes of Preterm Infants: Morbidity Replaces Mortality. *Clin. Perinatol.* **38**, 441–454 (2011).
36. Bright, H. R. et al. Neurocognitive Outcomes at 10 Years of Age in Extremely Preterm Newborns with Late-Onset Bacteremia. *J. Pediatr.* **187**, 43–49.e1 (2017).
37. Hedderich, D. M. et al. Hippocampal subfield volumes are non-specifically reduced in premature-born adults. *Hum. Brain Mapp.* **41**, 5215–5227 (2020).
38. Anand, K. & Dhikav, V. Hippocampus in health and disease: An overview. *Ann. Indian Acad. Neurol.* **15**, 239 (2012).
39. Skiöld, B. et al. Neonatal Magnetic Resonance Imaging and Outcome at Age 30 Months in Extremely Preterm Infants. *J. Pediatr.* **160**, 559–566.e1 (2012).
40. Back, S. A. & Miller, S. P. Brain injury in premature neonates: A primary cerebral dysmaturation disorder? *Ann. Neurol.* **75**, 469–486 (2014).
41. Gopalakrishnan, G. et al. Lipidome and proteome map of myelin membranes. *J. Neurosci. Res.* **91**, 321–334 (2013).
42. Lewis, K. T., Maddipati, K. R., Naik, A. R. & Jena, B. P. Unique Lipid Chemistry of Synaptic Vesicle and Synaptosome Membrane Revealed Using Mass Spectrometry. *ACS Chem. Neurosci.* **8**, 1163–1169 (2017).
43. Olsen, A. S. B. & Færgeman, N. J. Sphingolipids: membrane microdomains in brain development, function and neurological diseases. *Open Biol.* **7**, 170069 (2017).
44. Lauwers, E., Goodchild, R. & Verstreken, P. Membrane Lipids in Presynaptic Function and Disease. *Neuron* **90**, 11–25 (2016).
45. Tulodziecka, K. et al. Remodeling of the postsynaptic plasma membrane during neural development. *MBoC* **27**, 3480–3489 (2016).
46. Martínez, M. & Mougan, I. Fatty Acid Composition of Human Brain Phospholipids During Normal Development. *J. Neurochem.* **71**, 2528–2533 (1998).
47. Rodriguez-Navas, C., Morselli, E. & Clegg, D. J. Sexually dimorphic brain fatty acid composition in low and high fat diet-fed mice. *Mol. Metab.* **5**, 680–689 (2016).
48. Fitzner, D. et al. Cell-Type- and Brain-Region-Resolved Mouse Brain Lipidome. *Cell Rep.* **32**, 108132 (2020).
49. Satoi, H. et al. Astroglial expression of ceramide in Alzheimer's disease brains: A role during neuronal apoptosis. *Neuroscience* **130**, 657–666 (2005).
50. Van Doorn, R. et al. Fingolimod attenuates ceramide-induced blood–brain barrier dysfunction in multiple sclerosis by targeting reactive astrocytes. *Acta Neuropathol.* **124**, 397–410 (2012).
51. De Wit, N. M. et al. Astrocytic ceramide as possible indicator of neuroinflammation. *J. Neuroinflamm.* **16**, 48 (2019).
52. Lee, J. A., Hall, B., Allsop, J., Alqarni, R. & Allen, S. P. Lipid metabolism in astrocytic structure and function. *Semin. Cell Develop. Biol.* **112**, 123–136 (2021).
53. Moll, T., Shaw, P. J. & Cooper-Knock, J. Disrupted glycosylation of lipids and proteins is a cause of neurodegeneration. *Brain* **143**, 1332–1340 (2020).
54. Landgraf, A. et al. Widespread discordance between mRNA expression, protein abundance and de novo lipogenesis activity in hepatocytes during the fed-starvation transition. *Preprint at* https://doi.org/10.1101/2025.04.15.649020 (2025).
55. Dickson, J. L., Chase, J. G., Pretty, C. G., Gunn, C. A. & Alsweiler, J. M. Hyperglycaemic Preterm Babies Have Sex Differences in Insulin Secretion. *Neonatology* **108**, 93–98 (2015).
56. O'Neal, R. M. & Koeppe, R. E. Precursors in vivo of glutamate, aspartate and their derivatives of rat brain. *J. Neurochem.* **13**, 835–847 (1966).

57. Van Den Berg, C. J., Kržalić, L. J., Mela, P. & Waelsch, H. Compartmentation of glutamate metabolism in brain. Evidence for the existence of two different tricarboxylic acid cycles in brain. *Biochem. J.* **113**, 281–290 (1969).
58. Rae, C. D. et al. Brain energy metabolism: A roadmap for future research. *J. Neurochem.* **168**, 910–954 (2024).
59. He, Q. et al. Acetate enables metabolic fitness and cognitive performance during sleep disruption. *Cell Metab.* **36**, 1998–2014.e15 (2024).
60. Späth, C., Sjöström, E. S., Ahlsson, F., Ågren, J. & Domellöf, M. Sodium supply influences plasma sodium concentration and the risks of hyper- and hyponatremia in extremely preterm infants. *Pediatr. Res* **81**, 455–460 (2017).
61. Segar, J. L. & Jetton, J. G. Fluid and electrolyte management in the neonate and what can go wrong. *Curr. Opin. Pediatr.* **36**, 198–203 (2024).
62. Mathew, R., Arun, P., Madhavarao, C. N., Moffett, J. R. & Namboodiri, M. A. A. Progress toward Acetate Supplementation Therapy for Canavan Disease: Glyceryl Triacetate Administration Increases Acetate, but Not N-Acetylaspartate, Levels in Brain. *J. Pharmacol. Exp. Therapeutics* **315**, 297–303 (2005).
63. Lee, J., Ellis, J. M. & Wolfgang, M. J. Adipose Fatty Acid Oxidation Is Required for Thermogenesis and Potentiates Oxidative Stress-Induced Inflammation. *Cell Rep.* **10**, 266–279 (2015).
64. Hughes, C. S. et al. Single-pot, solid-phase-enhanced sample preparation for proteomics experiments. *Nat. Protoc.* **14**, 68–85 (2019).
65. Wang, Y. et al. Reversed-phase chromatography with multiple fraction concatenation strategy for proteome profiling of human MCF10A cells. *Proteomics* **11**, 2019–2026 (2011).
66. Herbrich, S. M. et al. Statistical Inference from Multiple iTRAQ Experiments without Using Common Reference Standards. *J. Proteome Res.* **12**, 594–604 (2013).
67. Fabregat, A. et al. The Reactome Pathway Knowledgebase. *Nucleic Acids Res.* **46**, D649–D655 (2018).
68. Perez-Riverol, Y. et al. The PRIDE database at 20 years: 2025 update. *Nucleic Acids Res.* **53**, D543–D553 (2025).
69. Scafidi, J. et al. Age-Dependent Cellular and Behavioral Deficits Induced by Molecularly Targeted Drugs Are Reversible. *Cancer Res.* **78**, 2081–2095 (2018).
70. Hughes, R. N. The value of spontaneous alternation behavior (SAB) as a test of retention in pharmacological investigations of memory. *Neurosci. Biobehav. Rev.* **28**, 497–505 (2004).
71. Matyash, V., Liebisch, G., Kurzchalia, T. V., Shevchenko, A. & Schwudke, D. Lipid extraction by methyl-tert-butyl ether for high-throughput lipidomics. *J. Lipid Res.* **49**, 1137–1146 (2008).
72. Medina, J. et al. Omic-Scale High-Throughput Quantitative LC–MS/MS Approach for Circulatory Lipid Phenotyping in Clinical Research. *Anal. Chem.* **95**, 3168–3179 (2023).
73. Gouda, H. et al. Differential utilization of vitamin B12-dependent and independent pathways for propionate metabolism across human cells. *J. Biol. Chem.* **300**, 107662 (2024).
74. Lei, Z. et al. Spinal cord injury disrupts plasma extracellular vesicles cargoes leading to neuroinflammation in the brain and neurological dysfunction in aged male mice. *Brain Behav. Immun.* **120**, 584–603 (2024).
75. Oleson, B. J. et al. Early life changes in histone landscape protect against age-associated amyloid toxicities through HSF-1-dependent regulation of lipid metabolism. *Nat. Aging* **4**, 48–61 (2024).
76. Pang, Z. et al. MetaboAnalyst 6.0: towards a unified platform for metabolomics data processing, analysis and interpretation. *Nucleic Acids Res.* **52**, W398–W406 (2024).
77. Jones, J. Dysregulated Fatty Acid Metabolism Following Intermittent Hypoxemia-induced Neonatal Brain Injury is Rescued by Treatment with Acetate. *Mendeley Data* https://doi.org/10.17632/NZWVKR7VGJ.1 (2025).
78. Folch, J., Lees, M. & Sloane Stanley, G. H. A simple method for the isolation and purification of total lipides from animal tissues. *J. Biol. Chem.* **226**, 497–509 (1957).
79. Stellaard, F., ten Brink, H. J., Kok, R. M., van den Heuvel, L. & Jakobs, C. Stable isotope dilution analysis of very long chain fatty acids in plasma, urine and amniotic fluid by electron capture negative ion mass fragmentography. *Clin. Chim. Acta* **192**, 133–144 (1990).
80. ten Brink, H. J. et al. Pristanic acid and phytanic acid in plasma from patients with peroxisomal disorders: stable isotope dilution analysis with electron capture negative ion mass fragmentography. *J. Lipid Res* **33**, 41–47 (1992).
81. Lagerstedt, S. A. et al. Quantitative Determination of Plasma C8–C26 Total Fatty Acids for the Biochemical Diagnosis of Nutritional and Metabolic Disorders. *Mol. Genet. Metab.* **73**, 38–45 (2001).
82. Sud, M. et al. LMSD: LIPID MAPS structure database. *Nucleic Acids Res.* **35**, D527–D532 (2007).
83. Fahy, E., Sud, M., Cotter, D. & Subramaniam, S. LIPID MAPS online tools for lipid research. *Nucleic Acids Res.* **35**, W606–W612 (2007).
84. Conroy, M. J. et al. LIPID MAPS: update to databases and tools for the lipidomics community. *Nucleic Acids Res.* **52**, D1677–D1682 (2024).
85. Ellis, J. M., Wong, G. W. & Wolfgang, M. J. Acyl Coenzyme A Thioesterase 7 Regulates Neuronal Fatty Acid Metabolism To Prevent Neurotoxicity. *Mol. Cell. Biol.* **33**, 1869–1882 (2013).
86. Bowman, C. E. et al. The Mammalian Malonyl-CoA Synthetase ACSF3 Is Required for Mitochondrial Protein Malonylation and Metabolic Efficiency. *Cell Chem. Biol.* **24**, 673–684.e4 (2017).

Acknowledgements

This work was supported by the National Institutes of Health Grants: R01 NS125653 (JS and SS), R01 NS110808 (SS), R01 NS099461 (JS), and R01 NS111230 (SS). Additional support provided by NICHD Intellectual and Developmental Disabilities Research Center at Kennedy Krieger Institute: P50HD103538 (JS). The authors would like to thank Dr. Robert Cole and Jeremy Post of the Johns Hopkins Mass Spectrometry and Proteomics Facility for their assistance with the proteomics analysis. All MALDI-MSI experiments were performed in the Johns Hopkins Applied Imaging Mass Spectrometry (AIMS) Core. Digital PCR was performed by the Johns Hopkins University School of Medicine Genetic Resources Core Facility (RRID:SCR_018669). Total lipid fatty acid analyses were performed by the Peroxisomal Diseases Laboratory and the Biochemical Genetics Laboratory at Kennedy Krieger Institute with the assistance of Shaghayegh Zokaei and Suzette Huguenin. We are deeply grateful to the families who generously donated brain tissue samples for the study. Human tissue was obtained from the NIH NeuroBioBank at the University of Maryland, Baltimore, MD with the assistance of Robert M. Johnson. The authors would like to thank Dr. Paul Watkins for discussion and critical review of the experimental design and manuscript.

Author contributions

R.F.F., S.S., and J.S. designed all experiments; R.F.F., S.S., and J.S. performed metabolic studies. J.S. performed behavioral experiments. RFF analyzed proteomics data provided by the Johns Hopkins Mass Spectrometry and Proteomics Facility. W.F., A.B.M., and S.S. measured total fatty acids by GC/MS, and RFF helped analyze data. Y.J. and J.W.J. performed lipidomic profiling by LC/MS/MS. CCJ, CMT, and KG performed the MALDI-MSI experiments, and CCJ and RFF performed the *m/z* lipid identification. R.A. assisted with metabolic studies; MJW provided CPT2 transgenic mouse and contributed to data interpretation. S.S. and J.S. supervised the entire project; R.F.F., S.S., and J.S. wrote the manuscript. All authors critically revised the manuscript and approved the final version.

Competing interests

The authors declare no competing interests.

Additional information

Supplementary information The online version contains supplementary material available at https://doi.org/10.1038/s41467-025-67542-6.

Correspondence and requests for materials should be addressed to Susanna Scafidi or Joseph Scafidi.

Peer review information *Nature Communications* thanks Richard Bazinet who co-reviewed with Mackenzie SmithPatrycja Puchalska, and the other, anonymous, reviewer(s) for their contribution to the peer review of this work. A peer review file is available.